

## Recent Advances in Constructing Three-Dimensional Graphitic Carbon Nitride Based Materials and Their Applications in Environmental Photocatalysis, Photo-Electrochemistry, and Electrochemistry

W. Xia<sup>1</sup>, X. Li<sup>1</sup>, M. Cheng<sup>1</sup>, W. P. Xiong<sup>1</sup>, B. Song<sup>1</sup>, Y. Liu<sup>1</sup>, Y. Yang<sup>1</sup>, W. J. Wang<sup>1</sup>, S. Chen<sup>1</sup>, G. M. Zeng<sup>1\*</sup>, and C. Y. Zhou<sup>1\*</sup>

<sup>1</sup>College of Environmental Science and Engineering, Hunan University and Key Laboratory of Environmental Biology and Pollution Control (Hunan University), Ministry of Education, Changsha 410082, P.R. China

Received 03 September 2020; revised 20 February 2021; accepted 28 May 2021; published online 05 January 2024

**ABSTRACT.** Recently, graphitic carbon nitride ( $\text{g-C}_3\text{N}_4$ ), a promising visible-light-driven semiconductor material, has received enormous attention for photocatalytic water splitting, organic pollutant degradation, and  $\text{CO}_2$  reduction. However, the photocatalytic activity of bulk  $\text{g-C}_3\text{N}_4$  is restricted due to the insufficient light adsorption, ineffective utilization of photogenerated charge carriers, and low specific surface area. Compared with bulk  $\text{g-C}_3\text{N}_4$ , the three-dimensional graphitic carbon nitride based materials (3D CNBMs) have outstanding physical and chemical characteristics, such as large specific area, plentiful active sites, and excellent electrical conductivity. This article reviews the latest achievements in 3D CNBMs, and presents the state-of-the-art advances in the synthetic methods of 3D CNBMs. Meanwhile, various applications of 3D CNBMs in photocatalysis, photo-electrochemistry, and electrochemistry are systematically reviewed and discussed. In addition, possible improvements and perspectives of 3D CNBMs are proposed. This review aims to summarize a panorama of the up-to-date processes of 3D CNBMs in environmental and energy applications and provide some innovative thoughts to accelerate the ground-breaking research and development of 3D CNBMs for a sustainable future.

**Keywords:** environmental or energy applications,  $\text{g-C}_3\text{N}_4$ , photo-electrochemistry, synthetic methods, three-dimensional

### 1. Introduction

Human beings rely heavily on fossil fuels like petroleum, coal, and natural gas in modern society, making environmental pollution, and energy shortage become the two most prominent global issues at present (Huang et al., 2019; Ji et al., 2020; Qin et al., 2020; Xie et al., 2020; Xing et al., 2020; Ye et al., 2020; Zhou et al., 2020d). Environmental protection and renewable energy development have become the key to the sustainable development of mankind. Photocatalysis technology, which can directly take advantage of solar energy, has the characteristics of mild reaction, low energy consumption, and no secondary pollution (Cheng et al., 2019; Ye et al., 2019; Zhao et al., 2019; Li et al., 2020; Wu et al., 2020). It is of great significance and practical research value to commercialize the photocatalysis technology in environmental remediation and energy conversion (Wang et al., 2014; Zhou et al., 2019b; He et al., 2020).

At present, conventional photocatalyst materials can be divided into single-component inorganic semiconductor photo-

catalysts (Nakamura et al., 2000; Scuderi et al., 2016; Di Mauro et al., 2017;), composite photocatalysts (Wang et al., 2016b; Golestanbagh et al., 2018), and metal photocatalysts (Sakthivel et al., 2004; Li et al., 2016; Cao et al., 2017). Inorganic semiconductor photocatalysts refer to metal oxides, metal sulfides, etc. Titanium dioxide ( $\text{TiO}_2$ ) is extensively studied owing to its chemical stability, non-toxicity, and low price (Zheng et al., 2010; Shi et al., 2019; Luo et al., 2020; Wang et al., 2020a). However, the application of  $\text{TiO}_2$  is limited due to its wide bandgap (3.0 ~ 3.2 eV over different phases). It can only absorb ultraviolet light accounting for a very low proportion of the sunlight, resulting in the low utilization of solar energy (Silva et al., 2011; Yan et al., 2017a). Cadmium sulfide ( $\text{CdS}$ ), as a kind of metal sulfide photocatalysts, has become a high performance photocatalyst material with wide wavelength absorption range and good carriers transportation capacity (Zhang et al., 2014b; Cheng et al., 2018). However, the chemical stability of  $\text{CdS}$  is poor. In the photocatalytic process, sulfur ion is easy to be oxidized by holes, which causes the simultaneous release of  $\text{Cd}(\text{II})$  into the system and then results in environmental pollution (He et al., 2017). Usually, two or more inorganic semiconductor materials are connected to form composite photocatalysts. Since the energy band structures of semiconductor materials are different, the composite photocatalyst can overcome the disadvantages of the low utilization rate of sunlight of single semiconductor materials (Huang et al., 2020a). Metal photocatalysts can be divided into photo-

\* Corresponding author. Tel.: +86 731-88822754; fax: +86 731-88823701.  
E-mail address: zgming@hnu.edu.cn (G. M. Zeng).

\* Corresponding author. Tel.: +86 731-88822754; fax: +86 731-88823701.  
E-mail address: zhouchengyun@hnu.edu.cn (C. Y. Zhou).

catalysts containing a single metal element and heteronuclear complex photocatalysts composed of two metals (e.g., Ru-Pd, Ru-Rh, etc) (Duan et al., 2020). Bismuth (Bi) is a heavy metal with low-radioactivity and low-toxicity. It is abundant on earth, only second to silver. It has a good development prospect in the fields of medicine, organic synthesis, and catalysis. In the field of photocatalysis, most Bi-based photocatalysts are Bi(III) oxides, such as BiOCl, BiOBr, BiOI, Bi<sub>2</sub>WO<sub>6</sub>, BiPO<sub>4</sub>, Bi<sub>2</sub>O<sub>3</sub>, BiVO<sub>4</sub>, etc (Jiang et al., 2010; Ge et al., 2011; Ye et al., 2014; Li et al., 2018a; Sánchez-Rodríguez et al., 2018; Yi et al., 2019; Wang et al., 2020c). However, the poor utilization of visible light and the fast recombination of electron-hole pairs lead to unsatisfied photocatalytic performance (He et al., 2018b). Single-component silver-based semiconductor has high absorptivity to visible light and shows good catalytic activity in photocatalytic applications. Nevertheless, their poor stability and high price limit their practical applications (Huang et al., 2020b; Xue et al., 2020).

Wang et al. (2009a) successfully synthesized graphitic carbon nitride ( $\text{g-C}_3\text{N}_4$ ), a non-metal conjugate semiconductor composed of nitrogen and carbon elements, which could split water into hydrogen and oxygen after absorbing visible light. Graphitic carbon nitride has the advantage of distinguished energy band, remarkable physicochemical stability, facile synthesis, and environmental friendliness (Ong et al., 2016; Yang et al., 2020b). Specifically, it has a graphene-like planar structure, which composed of tri-s-triazine units by deamination. The bandgap of  $\text{g-C}_3\text{N}_4$  (2.7 eV) is narrower than that of  $\text{TiO}_2$ , which means that  $\text{g-C}_3\text{N}_4$  can utilize part of visible light in the photocatalytic reactions. Furthermore,  $\text{g-C}_3\text{N}_4$  has high heat-resistance and can stably exist in acid and alkali conditions. It can be simply fabricated by thermal polymerization with economical nitrogen-rich precursors (such as dicyandiamide, thiourea, melamine and urea) (Yan et al., 2009; Yang et al., 2020d). However, bulk  $\text{g-C}_3\text{N}_4$  usually shows unsatisfied photocatalytic performance owing to its low specific surface area, insufficient absorption to solar energy, and high possibility of recombination of photo-electron-hole (Zhang et al., 2016b; Khan et al., 2018; Yang et al., 2019; Wang et al., 2020a).

In order to enhance the photocatalytic activity of  $\text{g-C}_3\text{N}_4$ , researchers have carried out extensive studies. The modification methods mainly include element doping (Wang et al., 2009b; Zhang et al., 2014a; Wang et al., 2015a; Zhou et al., 2020b), heterojunction construction (Dong et al., 2013; Li et al., 2017) and morphological control (Yang et al., 2015; Shakeel et al., 2019; Wang et al., 2021a). Element doping is to control the energy band structure of  $\text{g-C}_3\text{N}_4$  by doping with homo-elements or hetero-elements. It can be divided into metal doping and non-metal doping. When metal elements are doped into  $\text{g-C}_3\text{N}_4$ , they act as electron acceptors that can enhance the ability of  $\text{g-C}_3\text{N}_4$  to capture photogenerated charge carriers. In addition, they can accelerate the separation and transfer of electron-hole pairs. Kamila Kočí et al. (2020) deposited platinum (Pt) nanoparticles on the  $\text{C}_3\text{N}_4$  catalyst surface (Pt /  $\text{C}_3\text{N}_4$ ). Due to the strong electronic acceptance of Pt nanoparticles, the photocatalytic quantum efficiency of Pt /  $\text{C}_3\text{N}_4$  catalyst was improved significantly. Non-metal doping changes the electronic structure of  $\text{g-C}_3\text{N}_4$  with electronegativity properties of non-metal elements (B, O,

I, P, S, etc.). Hu et al. (2020) doped iodine (I) into the open framework of  $\text{g-C}_3\text{N}_4$  (iodine-doped  $\text{g-C}_3\text{N}_4$ , CNIX). The characterization results showed that the response range of  $\text{g-C}_3\text{N}_4$  to visible light was expanded and the efficiency of photogenerated charge separation was improved. Heterojunction construction refers to the combination of semiconductors with different energy band structures, which is conducive to the transfer and separation of electron-holes as well as the broadening of the light absorption range. Yang (2020a) obtained the ultra-thin 2D / 2D  $\text{Ti}_3\text{C}_2$  /  $\text{g-C}_3\text{N}_4$  photocatalyst by calcining the mixture of  $\text{Ti}_3\text{C}_2$  particles and urea. The formation of heterojunction enabled a close interface contact between  $\text{Ti}_3\text{C}_2$  and  $\text{g-C}_3\text{N}_4$ . The  $\text{CO}_2$  photoreduction activity on  $\text{g-C}_3\text{N}_4$  coupling with  $\text{Ti}_3\text{C}_2$  was soaringly enhanced compared with pure  $\text{g-C}_3\text{N}_4$ .

The photocatalytic activities of catalyst materials are closely related to their morphology and structure (Wang et al., 2020b). To a certain extent, the physical and chemical properties are determined by the morphological structure and dimension of the catalyst, which further affect its photocatalytic activities. Therefore, controlling the morphology and structure could be an effective way to improve the performance of  $\text{g-C}_3\text{N}_4$ . Due to the layered structure of  $\text{g-C}_3\text{N}_4$ , two-dimensional (2D)  $\text{g-C}_3\text{N}_4$  can be acquired from the bulk  $\text{g-C}_3\text{N}_4$  by means of calcination, sonication, alkali exfoliation, etc. Zhou et al. (2020c) conducted heat treatment on  $\text{g-C}_3\text{N}_4$  and obtained ultra-thin macro-mesoporous carbon nitride nanosheets (denoted as mMCNNS) (Figures 1a-1f). Bulk  $\text{g-C}_3\text{N}_4$  can also be made into one-dimensional (1D)  $\text{g-C}_3\text{N}_4$  materials (like nanotubes, nanowires, nanorods, and so on.) with different lengths and diameters through mesoporous molecular sieves, silica, and other templates. Zheng et al. (2014) synthesized  $\text{g-C}_3\text{N}_4$  with helical rod-like morphology (named HR-CN) by using mesoporous silica as a sacrificial template (shown in Figure 1g).

Compared with 1D / 2D  $\text{g-C}_3\text{N}_4$ , the three-dimensional  $\text{g-C}_3\text{N}_4$  based materials (3D CNBMs) have a larger specific surface area and higher porosity. 3D CNBMs with a three-dimensional (3D) network have many superiorities in the catalytic applications. The huge specific surface area can greatly increase the number of active sites for adsorption and degradation of pollutants. Sunlight can form multiple reflections in the 3D framework to enhance the light absorption efficiency (Liu et al., 2021; Wang et al., 2021b). The 3D structure can efficiently prevent the agglomeration of catalysts and improve the stability of catalysts. It can improve the porosity, provide a porous channel for the transmission of electrons, and greatly improve the catalytic activities (Zhang et al., 2021; Zhao et al., 2021). The catalyst fixed in a 3D framework is easy for recycling. According to Figure 2, there has been a great increase in the number of publications and citations of 3D CNBMs since 2009.

This review accentuates an overview of the recent development and progress of 3D CNBMs. Other reviews on 3D  $\text{g-C}_3\text{N}_4$  classified and summarized the synthesis methods from the perspective of synthesis pathways (Li et al., 2019). In this work, the synthesis methods are systematically discussed from the aspect of 3D  $\text{g-C}_3\text{N}_4$  and 3D CNBMs respectively. This review not only discusses the application of 3D CNBMs as photocatalytic materials but also introduces the applications in photo-electro-

chemistry and electrochemistry as supplementary. Finally, possible improvements and perspectives of 3D CNBMs are proposed.

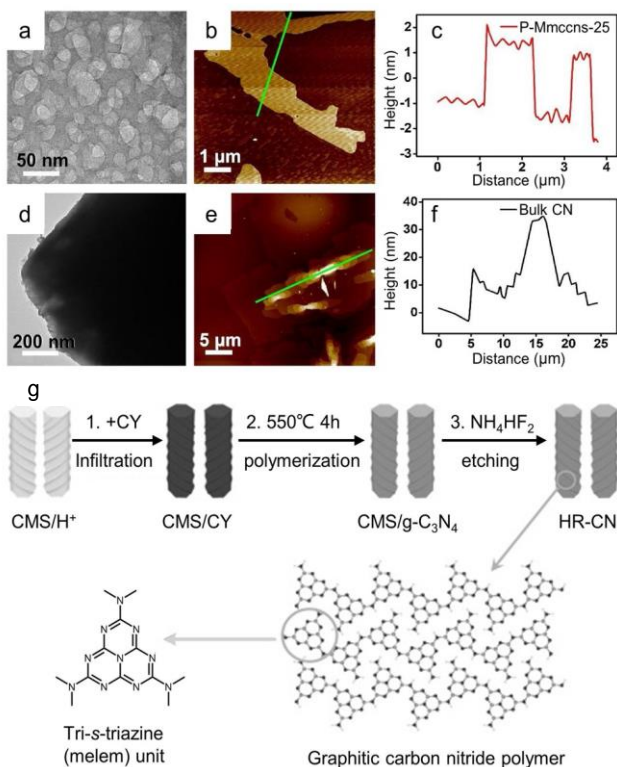


**Figure 1.** (a)-(d) HRTEM image, (b)-(e) AFM image and (c)-(f) corresponding height image of P-mMCNNS-25 and bulk CN (Zhou et al., 2020c). Copyright © 2020 Elsevier. (g) Synthetic process of graphitic carbon nitride (Zheng et al., 2014). Copyright © 2014 WILEY-VCH Verlag GmbH & Co. KGaA, Weinheim.

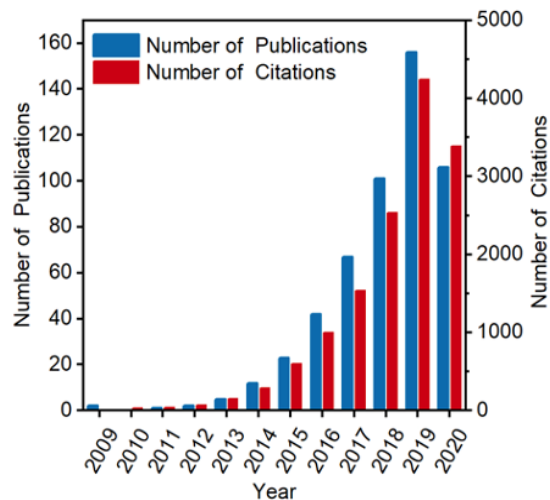


**Figure 2.** The annual collections of journal publications and citations concerning “graphitic carbon nitride” or “g-C<sub>3</sub>N<sub>4</sub>”, and “3D” or “three-dimensional” subjects since 2009. Adapted from ISI Web of Science, dated 17th July 2020.

## 2. The Synthetic Method of Three-Dimensional Graphitic Carbon Nitride

The performance of the target materials is not only dependent on the precursors, but also largely contingent on the synthesis methods. This section creatively summarizes the synthesis methods from the perspective of three-dimensional carbon nitride materials, including hard template method, soft template method, and self-template method (Table 1).

### 2.1. Hard Template Method

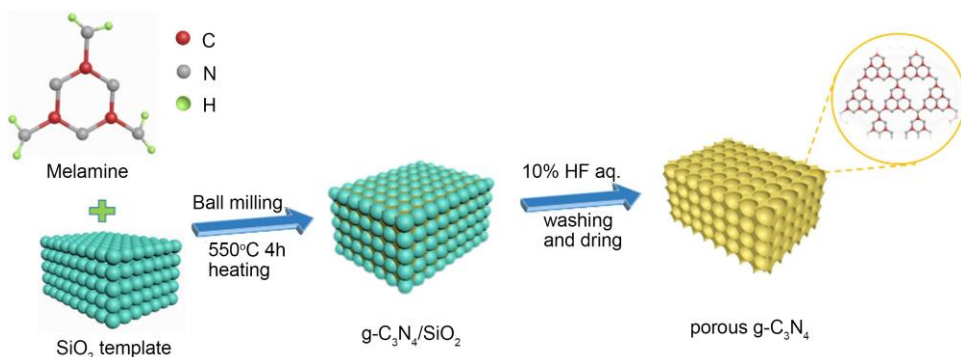
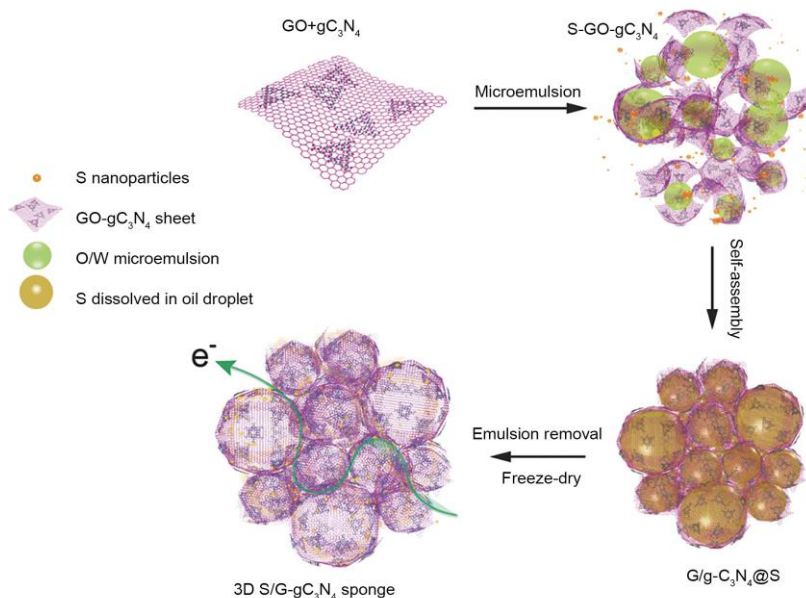
Hard template method mostly uses rigid materials connected by covalent bonds as templates to regulate the morphology and size of materials. Chen et al. (2020) used SiO<sub>2</sub> spheres as templates, mixed it with melamine, and heated them in a covered crucible. In this process, melamine was mixed with SiO<sub>2</sub> to form g-C<sub>3</sub>N<sub>4</sub>@SiO<sub>2</sub> with a core-shell structure, and then the mixture was washed by a hydrofluoric acid solution to remove the silica template (Figure 3). In 2016, Tomer et al. (2016) used three-dimensional mesoporous SiO<sub>2</sub> as a hard template and designed a mesoporous Ag-loaded g-C<sub>3</sub>N<sub>4</sub>. The results showed that the 3D mesoporous structure generated a large number of active sites, and accelerated the transfer of charge carriers. With the load of appropriate amount of Ag nanoparticles, the photocurrent response was further increased to four times. Due to the high stability of hard templates, the size and morphology of nanomaterials can be controlled by this method, which can be used for mass production. Whereas toxic chemicals are needed to be removed from the templates in the end, as they can easily cause environmental pollution. Additionally, in the process of template removal, the pore structure may collapse, which can easily cause damage to the porous structure and affect the photocatalytic performance of the material (Xie et al., 2016).

### 2.2. Soft Template Method

Soft template method means that the free precursors are assembled regularly to form a collective with different spatial structures under the action of intermolecular force and spatial limitation ability. The common soft templates used to fabricate 3D CNBMs include microemulsion, biological molecule, bubble template, ionic liquid, etc (Mohamed et al., 2018; Zhang et al., 2018a; Qi et al., 2019; Tang et al., 2019; Zhao et al., 2020). Zhang et al. (2018) used oil emulsion droplets containing dissolved sulfur as a soft template to form materials with large pores. The templates were covered with GO-g-C<sub>3</sub>N<sub>4</sub> sheets to assemble 3D porous sulfur/graphene@g-C<sub>3</sub>N<sub>4</sub> (S/GCN). As the emulsion evaporated, the sulfur was uniformly “glued” to the walls of the g-C<sub>3</sub>N<sub>4</sub> and wrapped inside at the same time. The microemulsion packaging method successfully obtained g-C<sub>3</sub>N<sub>4</sub> cathode with sulfur content up to 82 wt% (Figure 4). Mohamed et al. (2018) designed and synthesized 3D porous microtubule carbon-doped g-C<sub>3</sub>N<sub>4</sub> with kapok fiber (t-KF) as the biological molecule template by a simple thermal condensation method. T-KF served as both a biological template and an in-situ carbon dopant. The key to bubble templates is to form bubbles that prevent particles from sticking together. Tang et al. (2019) used ammonium

**Table 1.** The Synthetic Method of Three-Dimensional Graphitic Carbon Nitride

Methods	Pros	Cons	Template	Average Pore Sizes (nm)	BET Surface Area (m <sup>2</sup> /g)	References
Hard template method	Easy to control size and morphology	Cause contamination	SiO <sub>2</sub>	12.40	159.70	(Chen et al., 2020)
			mesoporous SiO <sub>2</sub>	5.20	170.80	(Tomer et al., 2016)
Soft template method	Do not need to remove the template	Poor stability compared with hard template method	kapok fiber	27.80	49.60	(Mohamed et al., 2018)
			NH <sub>3</sub> and HCl gases	N/A	103.10	(Tang et al., 2019)
			ionic liquid	15.00	381.00	(Zhao et al., 2020)
			NaCl	N/A	33.60	(Ai et al., 2019)
Self-template method	Easy to operation, low cost, and low pollution	Not well known	cyanuric acid melamine d-supramolecular Melamine-cyanuric acid-urea supramolecular melamine-cyanuric acid supramolecular	20.00 18.19 N/A	130.00 42.15 58.50	(Chen et al., 2019) (Gu et al., 2020) (Zhou et al., 2019a)

**Figure 3.** Schematic illustration of the 3D porous g-C<sub>3</sub>N<sub>4</sub> fabrication procedures(Chen et al., 2020). Copyright © 2020 Elsevier.**Figure 4.** The procedure for preparing S/GCN hybrid sponge (Zhang et al., 2018a). Copyright © 2018 WILEY-VCH Verlag GmbH & Co. KGaA, Weinheim.

chloride ( $\text{NH}_4\text{Cl}$ ) as a gas template to synthesize ultra-thin bubble-like  $\text{g-C}_3\text{N}_4$  materials. In the synthetic process,  $\text{NH}_4\text{Cl}$  was decomposed into gaseous  $\text{NH}_3$  and  $\text{HCl}$  after heating, and these gases aggregated on  $\text{g-C}_3\text{N}_4$  to fabricate bubble modes. At the same time, the bubble molds expanded under the action of hot air, further preventing the inter-layer accumulation of  $\text{g-C}_3\text{N}_4$ . The self-assembly behavior of ionic liquids and the properties that they can form hydrogen bonds affect the structure of carbon nitride aggregates. Zhao et al. (2020) successfully prepared 3D mesoporous carbon nitride materials by decomposing ionic liquid (1-butyl-3-vinylimidazolium bromide) and precursor (cyanurate-melamine supramolecular aggregate) under high-temperature calcination. Compared with the conventional template

method, the salt template directly adopts the soluble salt as the template which can effortlessly be removed by immersing in water. Ai et al. (2019) tuned the 3D porous structure of carbon nitride through sodium chloride ( $\text{NaCl}$ ) templates.  $\text{NaCl}$  introduced metal ligands as donors and cyano groups as acceptors to participate in the construction of internal donor-acceptor (D-A) heterostructures, greatly promoting the separation of carriers. According to the experiment, the photocurrent density of  $\text{MnO}_x$ -decorated 3D porous  $\text{C}_3\text{N}_4$  was nearly triple than that of bulk  $\text{g-C}_3\text{N}_4$ . Applying the soft template method does not need to remove the template. While materials synthesized by soft template method generally have poor stability compared with hard template method.

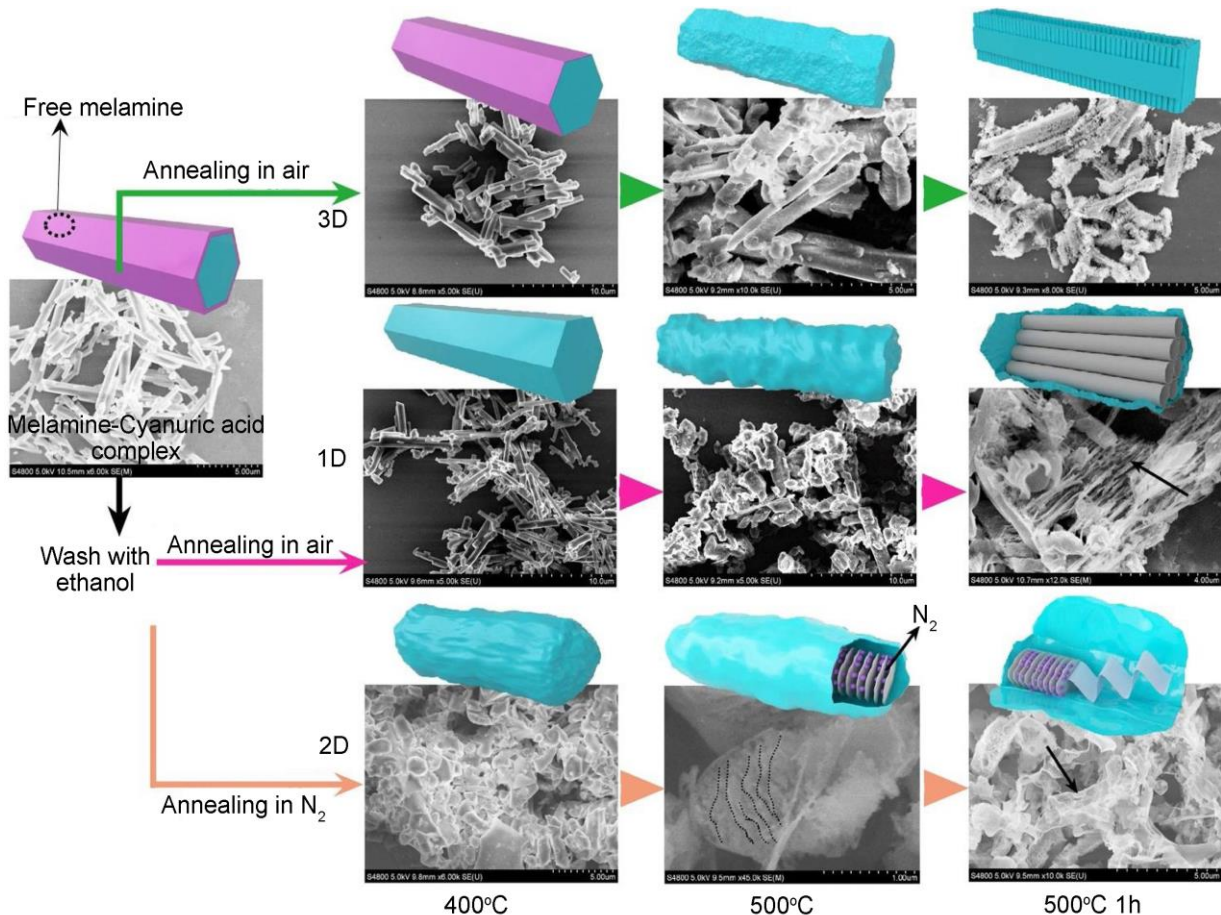


**Figure 5.** Fabrication process of  $\text{g-C}_3\text{N}_4$  with different structure (Zhou et al., 2019a). Copyright © 2019 Elsevier.

### 2.3. Self-Template Method

Molecular self-assembly is a method to assemble monomers (such as melamine, cyanuric acid, barbiturate, or derivatives) into supramolecular aggregates by hydrogen bonds, Van Der Waals Forces, or electrostatic interaction for controlling structures (Tian et al., 2014; Zhang et al., 2015; Huo et al., 2018). This method has the characteristics of simple operation, low cost, and low pollution. Chen et al. (2019) synthesized 3D  $\text{g-C}_3\text{N}_4$  by a simple self-template method. In this synthetic process, melamine and

cyanuric acid were dissolved in water and then self-assembled to a 3D network of cyanurate-melamine supramolecular precursors. Then, a pale-yellow 3D  $\text{g-C}_3\text{N}_4$  sample was produced by polycondensation at high temperatures. The 3D framework was assembled from highly crystalline ultrathin nanosheet units, providing a pathway for faster carrier transport. In addition, 3D  $\text{g-C}_3\text{N}_4$  maintained stability for more than 100 h in the whole water decomposition reaction thanks to its 3D structure that prevented the agglomeration of nanomaterials. Gu et al. (2020)

synthesized 3D porous g-C<sub>3</sub>N<sub>4</sub> by supramolecular self-assembly of melamine, cyanuric acid and urea under appropriate conditions, and used this material as a carrier to load ammonium vanadate (V-IL/3D g-C<sub>3</sub>N<sub>4</sub>) for aerobic oxidation and desulfurization by a thermal solvent method. Based on the characterization results, the BET surface area of ammonium vanadate (V-IL) was greatly increased as it was uniformly loaded on the 3D porous

g-C<sub>3</sub>N<sub>4</sub>, thus exposing more active sites. By changing the heat treatment conditions, the geometric size and morphological structure of carbon nitride can be controlled. Zhou et al. (2019a) used melamine and cyanuric acid as precursors and set different heat treatment parameters. They successfully obtained graphitic carbon nitride with a 3D towel gourd structure, a 2D nanosheet structure, and a 1D nanotube structure, respectively (Figure 5).

**Table 2.** The Synthetic Method of Three-Dimensional Graphitic Carbon Nitride Based Materials

Methods	Prons	Cons	Catalyst	Average pore Sizes (nm)	BET surface area (m <sup>2</sup> /g)	References
In-situ grown	Thermal polymerization	Wide applicability	High energy consumption	g-C <sub>3</sub> N <sub>4</sub> /MgO g-C <sub>3</sub> N <sub>4</sub> /NiO WC <sub>1-x</sub> /g-C <sub>3</sub> N <sub>4</sub>	14.44 N/A N/A	83.37 123.60 99.70
		Freeze-drying	Good control over morphology and high structure stability	g-C <sub>3</sub> N <sub>4</sub> /cellulose	N/A	128.97
		Heat-cooling	Easy to operation	g-C <sub>3</sub> N <sub>4</sub> -agar	N/A	38.04
Hydrothermal/solvent-thermal		Mild reaction conditions and less hard agglomeration	Depend on the reaction equipment and produce waste liquid	g-C <sub>3</sub> N <sub>4</sub> /SnS <sub>2</sub> g-C <sub>3</sub> N <sub>4</sub> /α-Fe <sub>2</sub> O <sub>3</sub> CdS/ g-C <sub>3</sub> N <sub>4</sub>	N/A N/A N/A	51.40 119.60 22.23
						(Zhou et al., 2018) (Wang et al., 2019a) (Xiong et al., 2019) (Bai et al., 2020) (Tan et al., 2019) (Sun et al., 2014) (Kim et al., 2020) (Liu et al., 2020)

### 3. The Synthetic Method of Three-Dimensional Graphitic Carbon Nitride Based Materials

By adding other components in the process of material synthesis can overcome the poor performance of single-component photocatalysts. This section summarizes the synthesis methods of 3D graphitic carbon nitride based composite materials, which are mainly divided into thermal polymerization, freeze-drying, heat-cooling, hydrothermal / solvent-thermal, etc (Table 2).

#### 3.1. In-Situ Growth

##### 3.1.1. Thermal Polymerization

Thermal polymerization is a method in which molecular monomers condense into graphitic carbon nitride polymers under thermal calcination (Zhou et al., 2020b). Because of the small specific surface area, pure graphitic carbon nitride is often modified with other materials to produce 3D CNBs composites. Zhou et al. (2018) simply calcined the mixed solution of melamine and MgCl<sub>2</sub> to obtain a three-dimensional g-C<sub>3</sub>N<sub>4</sub> / MgO composite photocatalyst. It has abundant adsorption sites, a three-dimensional network structure, and a rough surface morphology. Wang et al. (2019a) prepared spherical flower-shaped g-C<sub>3</sub>N<sub>4</sub> / NiO heterojunction composites by calcination and hydrothermal methods. In the synthetic process, g-C<sub>3</sub>N<sub>4</sub> was obtained through the first calcination, and then the obtained g-C<sub>3</sub>N<sub>4</sub> was mixed with nickel nitrate and urea, and transferred to the sealed high-pressure reactor for 12 hours. The three-dimensional spherical flower g-C<sub>3</sub>N<sub>4</sub> / NiO composite photocatalysts were obtained after the second calcination. G-C<sub>3</sub>N<sub>4</sub> was composed of smooth flat nanosheets with a layered structure, while pure NiO had a spherical

structure. After the hydrothermal reaction, the different nanosheets were assembled and combined with NiO, resulting in the formation of coarse and dense “petals” (g-C<sub>3</sub>N<sub>4</sub>) on the NiO surface. Three-dimensional flower-shaped g-C<sub>3</sub>N<sub>4</sub>/NiO exhibited a larger BET surface area than pure g-C<sub>3</sub>N<sub>4</sub> and pure NiO, which were 2.06 and 2.12 times respectively. Xiong et al. (2019) firstly synthesized hexacarbonyl tungsten / melamine composite precursors with W(CO)<sub>6</sub> and melamine as the initial reactants by sonochemical method. Then, the final product of g-C<sub>3</sub>N<sub>4</sub> / WC<sub>1-x</sub> was obtained after calcination step by step (shown in Figure 6). The first 8 h calcination in Ar / H<sub>2</sub> mixed atmosphere was to promote the pyrolysis of tungsten-based compounds and the condensation of melamine. The second step was to induce the formation of nitrogen defects to form g-C<sub>3</sub>N<sub>x</sub> / WC<sub>1-x</sub> (g-C<sub>3</sub>N<sub>4</sub> for nitrogen defects is labeled g-C<sub>3</sub>N<sub>x</sub>). In the whole pyrolysis process, 2D WC<sub>1-x</sub> / g-C<sub>3</sub>N<sub>4</sub> nanosheet was spontaneously combined into a three-dimensional structure.

##### 3.1.2. Freeze-Drying

Freeze-drying is mainly used to obtain the aerogels with 3D porous structure. In this process, water goes through two-phase transitions. First, water solidifies from liquid water into solid water (i.e., ice crystal), and then the solid water sublimates into gaseous water. Loose and porous materials can be obtained by this method as the water is directly sublimated from the ice crystals into the gaseous phase and escapes out. The dried materials replicate the ice crystal structure without condensation and collapse, which can effectively avoid the destruction of the original structure morphology. Wan et al. (2016) obtained the C<sub>3</sub>N<sub>4</sub> / graphene oxide macroscopic aerogel (C<sub>3</sub>N<sub>4</sub> / GOA) composites

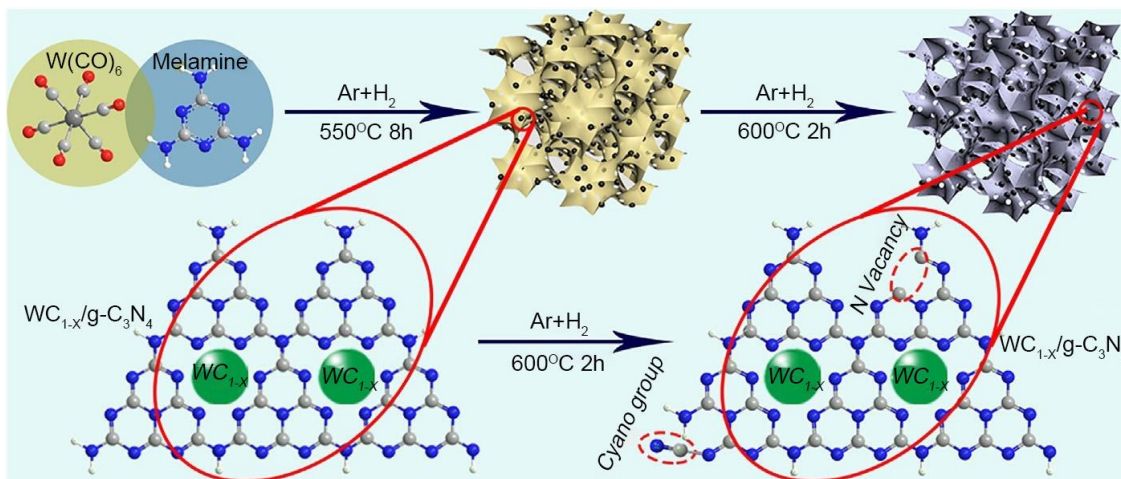


**Figure 6.** The synthesis procedure of  $\text{g-C}_3\text{N}_4/\text{WC}_{1-x}$  composites (Xiong et al., 2019). Copyright © 2019 WILEY-VCH Verlag GmbH & Co. KGaA, Weinheim.

by freeze-drying the prepared  $\text{C}_3\text{N}_4$  and GO suspension for 48 h. During this process, the 2D layered powder was successfully integrated into the 3D macro photocatalyst (Figure 7). The results showed that the  $\text{C}_3\text{N}_4/\text{GOA}$  composites had excellent photoelectric chemistry (PEC) performance, photocatalytic activity, and high adsorption capacity. Yan et al. (2017b) reported a simple method for synthesizing 3D  $\text{Cu}_2\text{O}/\text{g-C}_3\text{N}_4/\text{RGO}$  aerogel. The prepared  $\text{g-C}_3\text{N}_4$  and  $\text{Cu}_2\text{O}$  were mixed with GO solution and kept at 95 °C for the organization of 3D hydrogel. Then, 3D aerogel was obtained by freeze-drying at -56 °C for 12 h. The ternary aerogels exhibited a 3D porous network structure and excellent photocatalytic performance. Additionally, this composite photocatalyst could be simply removed only by tweezers and the photocatalytic activity basically remained unchanged after recycling use for many times. Bai et al. (2020) added  $\text{g-C}_3\text{N}_4$  into the cellulose solution, and then processed it by ultrasound to form a uniform mixture. Under the action of N, N'-methylenebis (acrylamide) (MBA, cross-linking agent),  $\text{g-C}_3\text{N}_4$  was combined with cellulose to form hydrogels. Finally, 3D  $\text{g-C}_3\text{N}_4/\text{cellulose}$  (CN / CE) aerogels with high porosity were ob-

tained by freeze-drying. The 3D framework not only provided mechanical support but also prevented the agglomeration of  $\text{g-C}_3\text{N}_4$ . Moreover, the large number of pores promoted mass transfer in reaction.

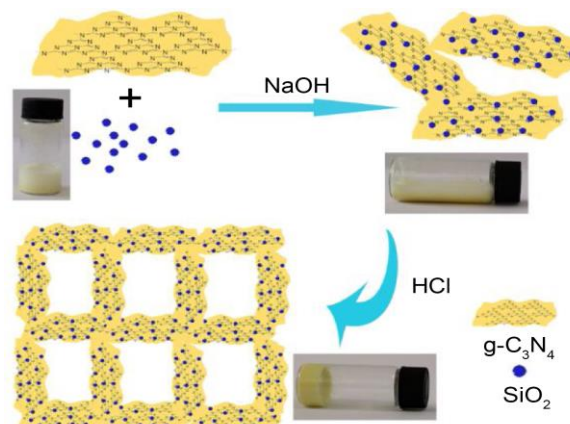


**Figure 8.** The synthesis procedure of  $\text{C}_3\text{N}_4$ -agar hydrogel (Zhang et al., 2016b). Copyright © 2016 Elsevier.

### 3.1.3. Heat-Cooling

Heat-cooling means heating the precursors to a lower temperature and then cooling to ambient temperature after adding certain substances with thermally reversible properties. Zhang et al. (2016a) used agar to prepare hybrid hydrogels through its thermally reversible sol-gel transition properties. As shown in Figure 8, a certain proportion of agar and  $\text{g-C}_3\text{N}_4$  were put into water and treated by ultrasound for 30 min. The solution was heated to 95 °C and cooled in the air to room temperature to form  $\text{g-C}_3\text{N}_4$ -agar hybrid hydrogels. The heat-cooling polymerization process transformed agar and  $\text{g-C}_3\text{N}_4$  nanoparticle solution into a hybrid hydrogel with a 3D network structure. The agar hydrogel served as the link bridge of  $\text{g-C}_3\text{N}_4$  particles from

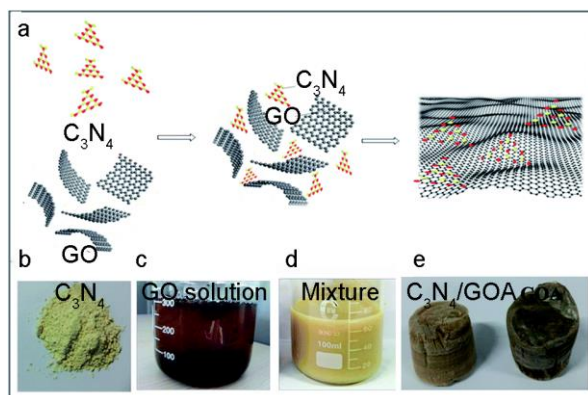


**Figure 7.** The synthesis procedure of  $\text{C}_3\text{N}_4/\text{GOA}$  (Wan et al., 2016). Copyright © 2016 Royal Society of Chemistry.

Transmission Electron Microscope (TEM) images. Tan et al. (2019) used agar and g-C<sub>3</sub>N<sub>4</sub> powder as raw materials to obtain g-C<sub>3</sub>N<sub>4</sub>-agar hybrid aerogel through the heat-cooling polymerization process. The g-C<sub>3</sub>N<sub>4</sub>-agar mixture aerogels showed improved light absorption and photocurrent response capability. Moreover, the 3D network structure not only showed excellent adsorption performance but also could overcome the difficulty in recycling the powder catalyst.

### 3.2. Hydrothermal / Solvent-Thermal

Hydrothermal / solvent-thermal refers to the preparation of composite materials by placing the precursor in water / solvent under high temperature and pressure. Sun et al. (2014) synthesized 3D flower-shaped g-C<sub>3</sub>N<sub>4</sub> / SnS<sub>2</sub> composites by hydrothermal method. This composites with heterojunction structure presented wider light absorption and faster photocurrent responses. Kim et al. (2020) prepared g-C<sub>3</sub>N<sub>4</sub> /  $\alpha$ -Fe<sub>2</sub>O<sub>3</sub> / graphene aerogels (CNFGA) by using graphene oxide (GO), g-C<sub>3</sub>N<sub>4</sub>, and FeCl<sub>3</sub> as

raw materials through a simple hydrothermal method (shown in Figure 9). FeCl<sub>3</sub> hydrolyzed and interacted with the oxygen groups on GO board via static electricity, forming FeOOH deposition on 2D GO. Then the mixture combined with g-C<sub>3</sub>N<sub>4</sub> nanosheets in an autoclave. In the process of hydrothermal, GO changed into reduced graphene oxide (rGO) and FeOOH changed into  $\alpha$ -Fe<sub>2</sub>O<sub>3</sub>. Liu et al. (2020) calcined melamine at 550 °C to obtain yellow powder g-C<sub>3</sub>N<sub>4</sub>, and then g-C<sub>3</sub>N<sub>4</sub> was added into isopropyl alcohol solution for sonication for 6 h. The CdS / g-C<sub>3</sub>N<sub>4</sub> composites were then synthesized through solvent-thermal reaction by using cadmium sulfate and thiourea as cadmium sources and sulfur sources respectively. This material not only had a 2D / 2D close contact interface but also had a 3D layered framework. The hydrothermal / solvent-thermal method is mild, which can avoid hard agglomeration in the calcination process. However, the reaction conditions of high temperature and high pressure make it depend on the reaction equipment. In addition, it is necessary to solve the problem of waste liquid caused by hydrothermal / solvent-thermal method.



**Figure 9.** The synthesis procedure of CNFGA (Kim et al., 2020). Copyright © 2020, John Wiley and Sons.

## 4. The Application of Three-Dimensional Graphitic Carbon Nitride Based Materials

### 4.1. Photocatalytic Applications

3D CNBMs have received enormous attention for water splitting, organic pollutants degradation, and CO<sub>2</sub> reduction in solar photocatalysis due to the large specific area, plentiful active sites, and excellent electrical conductivity. The detailed applications in photocatalysis are as follows.

#### 4.1.1. Organic Pollutants Degradation

3D CNBMs photocatalysts have been widely used in the degradation and mineralization of organic pollutants, mainly including dyes, antibiotics, pesticides, and so on (Yuan et al., 2016; Sheng et al., 2019; Wang et al., 2019b; Gupta et al., 2020; Si et al., 2020; Yang et al., 2020c;). The electrons in the valence band can be excited to the conduction band under the irradiation of solar energy, generating oxidative holes and reductive electrons to mineralize organic pollutants. The 3D structure of CNBMs can provide multi-dimensional transport channels, effectively promoting the separation and transfer of photo-generated electron-hole pairs, thereby greatly improving the photocatalytic performance.

In 2015, Zhang et al. (2015) applied 3D CNBMs in organic pollutants degradation for the first time. They hybridized

graphene / g-C<sub>3</sub>N<sub>4</sub> and Ag@AgVO<sub>3</sub> nanowires for the removal of methylene blue, promoting the possibility of the applications of 3D composites in environmental protection. After that, Li et al. (2018b) synthesized a highly efficient g-C<sub>3</sub>N<sub>4</sub> / TiO<sub>2</sub> / kaolinite composite, which exhibited high degradation ability to ciprofloxacin (CIP) and high disinfection ability towards *S. aureus*. The superoxide radical ( $\cdot$ O<sub>2</sub><sup>-</sup>) was proved to be the main active species in the procedure of CIP removal. Liu et al. (2019) discussed the influences of other antibiotics and water sources in evaluating photocatalytic performance of g-C<sub>3</sub>N<sub>4</sub> / Ag<sub>2</sub>CO<sub>3</sub> / graphene oxide (CN / AC / GO) composite to degrade tetracycline (TC). The composite material showed highly efficiency to the degradation of OTC-HCL and LVFX. The degradation rates of TC by CN / AC / GO in actual wastewater samples only slightly decreased, which indicated a good application potential in environmental remediation. Gupta et al. (2020) prepared atom-thin sulfur-doped g-C<sub>3</sub>N<sub>4</sub> / ZnO photocatalysts. This interconnected 3D porous structure consisted of 2D graphitic thin plates and ZnO nanoscale plates. Its degradation rate of CIP was up to 98%, which was 18 and 38% higher than that of ZnO and s-g-C<sub>3</sub>N<sub>4</sub>, respectively. Table S1 shows the applications of 3D CNBMs for degrading organic pollutants.

#### 4.1.2. Water Splitting for Hydrogen Production

Hydrogen is recognized as a clean energy source in the world.

In the absence of sacrificial agents, using solar energy as the driving force to split water into hydrogen and convert solar energy to hydrogen energy can effectively reduce human dependence on non-renewable energy sources such as fossil fuels and alleviate the energy crisis (Yan et al., 2011; Lu et al., 2014; Zhou et al., 2015; Fu et al., 2019). The core of semiconductor photocatalyst for photocatalytic total water splitting under the action of visible light lies in the bandgap of the catalyst and the position of the valence band and conduction band. Specifically, the top of the valence band must be more positive than the O<sub>2</sub> / H<sub>2</sub>O redox potential, and the bottom of the conduction band must be more negative than the H<sup>+</sup> / H<sub>2</sub> 0 V (vs. NHE) redox potential (Kudo et al., 2009). In theory, g-C<sub>3</sub>N<sub>4</sub> has the innate advantage of total water splitting. However, oxygen production is a complex four-electron reaction, so the photolysis of water is still dominated by hydrogen production (Liu et al., 2012).

Shen et al. (2014) synthesized a novel porous g-C<sub>3</sub>N<sub>4</sub> with high performance of visible-light photocatalytic H<sub>2</sub> evolution by using cyanuric acid. In their experiment, cyanuric acid was used as a polymerization inhibitor due to the strong hydrogen bond with melamine. Luo et al. (2018) proposed a simple method to generate 3D spongy g-C<sub>3</sub>N<sub>4</sub> via a combination treatment of acid protonation and thermal oxidation to bulk g-C<sub>3</sub>N<sub>4</sub>. Experimental results showed that these two treatments had a positive effect on the rate of hydrogen evolution. Qian et al. (2019) successfully synthesized 3D porous g-C<sub>3</sub>N<sub>4</sub>. The porous structure had many advantages, such as large specific surface area, highly efficient charge separation and fast electron transfer efficiency. Owing to this unique structure, the rate of hydrogen evolution catalyzed by porous g-C<sub>3</sub>N<sub>4</sub> was up to 598 mol·h<sup>-1</sup>·g<sup>-1</sup> and the apparent quantum yield at 420 nm was 3.31%. Zhou et al. (2020a) successfully synthesized thin-shell honeycomb g-C<sub>3</sub>N<sub>4</sub> (g-C<sub>3</sub>N<sub>4</sub>-TSH) with melamine and NH<sub>4</sub>Cl for photocatalytic hydrogen evolution. It has been certificated that the photoelectron migration distance had been diminished which boosted the mass transfer owing to its special thin-shell honeycomb structure. The apparent quantum efficiency was 9.86%, which was better than many reported modified g-C<sub>3</sub>N<sub>4</sub>. Table S2 shows the 3D CNBMs for H<sub>2</sub> production.

#### 4.1.3. CO<sub>2</sub> Reduction

Due to the over-reliance on fossil fuels in the modern industry, the emission of CO<sub>2</sub> is serious. The use of solar energy to convert CO<sub>2</sub> into green fuel is an environmentally friendly and energy-saving approach to deal with the global energy crisis and greenhouse effect. The process of CO<sub>2</sub> conversion is the reaction of CO<sub>2</sub> reduction by electrons (He et al., 2015; Wang et al., 2015b; Ye et al., 2015; Di et al., 2017; Fu et al., 2017).

Wang et al. (2018b) utilized 3D g-C<sub>3</sub>N<sub>4</sub> / C composites as photocatalysts for the reduction of CO<sub>2</sub>. Photocatalytic measurements indicated that these composites showed higher activity for CO<sub>2</sub> reduction with CO and CH<sub>4</sub> yield of 229 and 112 μmol·g<sup>-1</sup>. It is obvious that the improvement of photocatalytic performance was mainly because of the modification of its structure and the enhancement of light capture and better CO<sub>2</sub> adsorption capacity. Wang et al. (2018b) synthesized a new g-C<sub>3</sub>N<sub>4</sub> / BiFeWO<sub>x</sub> heterojunction photocatalyst by in-situ solvent-thermal method. In this way, a tight chemical bond interface

can be established between BiFeWO<sub>x</sub> and g-C<sub>3</sub>N<sub>4</sub>. Due to the interface interaction, g-C<sub>3</sub>N<sub>4</sub> / BiFeWO<sub>x</sub> heterojunction catalysts showed high visible light sensitivity and efficient carrier separation and transfer. Under visible light irradiation, the yield of CO production by CO<sub>2</sub> reduction (43 mol·h<sup>-1</sup>·g<sup>-1</sup>) was higher than that of pure BiFeWO<sub>x</sub> (5.2 mol·h<sup>-1</sup>·g<sup>-1</sup>) and g-C<sub>3</sub>N<sub>4</sub> (8.9 mol·h<sup>-1</sup>·g<sup>-1</sup>). Recently, Sun et al. (2020a) used template method and microwave method to load copper nanoparticles (Cu-NPS) on the special g-C<sub>3</sub>N<sub>4</sub> foam to obtain Cu / CF composite materials. On the one hand, the 3D porous structure of foam-shaped semicon-ductor photocatalyst provided gas transmission channel for CO<sub>2</sub> absorption and diffusion. On the other hand, 0D metal nanoparticles loaded on 3D semi-conductors formed a heterojunction, which inhibited the recombination of electron and hole and promoted photogenerated charge separation efficiency. Table S3 shows the applications of 3D CNBMs for CO<sub>2</sub> reduction.

#### 4.2. Photo-Electrochemical Applications

3D CNBMs, as excellent photosensitive materials, have the characteristics of strong light capture ability and high charge separation rate, which can be used in the photoelectrochemical analysis. Wen et al. (2020) synthesized cathode materials based on the synthesized three-dimensional ZnO / Au / g-C<sub>3</sub>N<sub>4</sub> heterojunction composites for photochemical water decomposition. The photocathode of ZnO / Au / g-C<sub>3</sub>N<sub>4</sub> loaded with platinum co-catalyst showed excellent hydrogen production rate and Faraday efficiency in the experiment. 3D CNBMs not only can be directly used in the fabrication of photocathodes but also can be the promising candidate in photoelectro-chemical sensors. Du and co-authors prepared a simple PEC sensor based on 3D branched crystalline carbon nitride (3D BC-C<sub>3</sub>N<sub>4</sub>) to detect traces of Cu<sup>2+</sup> in water (Du et al., 2020). The lowest detection concentration reached 0.38 nM, which was comparable to or even better than previously reported studies. Lv et al. (2020) synthesized F8BT / g-C<sub>3</sub>N<sub>4</sub> heterojunction with organic polymer semiconductor and used it as photosensitive material and constructed a sensitive PEC sensor for carcinoembryonic antigen (CEA) detection. The sensor showed good performance, such as satisfactory selectivity, acceptable accuracy, and high sensitivity, indicating the potential in cancer biomarkers.

#### 4.3. Electrochemical Applications

Oxygen reduction reaction (ORR) is the pivotal reaction in energy storage devices. At present, Platinum-based materials are the most efficient electrocatalysts in ORR. Hoverer, the expensive cost and limited availability have restricted the development (Gu et al., 2016; Wang et al., 2018c). 3D CNBMs are cheap materials with good physicochemical stability. They have a high content of nitrogen elements, which can be the potential sites to modify the electronic structures and the electroconductivity properties (Liu and Zhang, 2013; Tian et al., 2014). 3D CNBMs would be the potential materials to replace Pt-based electrocatalysts. Specifically, they can be used as ORR electrocatalyst in polymer electrolyte membrane fuel cell (PEMFC). Qin et al. (2014) designed and prepared mesoporous carbon nitride/graphene composites and used them as an electrocatalyst for ORR in PEMFC.

As a consequence of the hollow and mesoporous structure, this electrocatalyst showed remarkably strengthened electrocatalytic activity and excellent resistance in methanol, indicating a promising application prospect in PEMFC. Also, the 3D CNBMs bifunctional electrocatalysts with oxygen reduction / evolution reactions (ORR / OER) can be reasonably designed and prepared, which is particularly important for promoting the development of metal-air battery. Wu et al. (2017) designed and prepared ultrathin N-doped carbon / g-C<sub>3</sub>N<sub>4</sub> composites. The unique loofa-like 3D network structure of the material showed obvious ORR activity and excellent OER activity, which had great application potential in the production of bifunctional catalysts. Li and co-authors prepared cobalt catalyzed nitrogen-doped carbon nanotubes based on g-C<sub>3</sub>N<sub>4</sub> materials and applied this catalyst into self-made zinc-air batteries (Li et al., 2018c). This battery showed high specific capacity and excellent cycling stability. Additionally, 3D CNBMs are low-cost materials with excellent electrical conductivity, which supports vertical charge transfer during charging and discharging, and they have potential applications in supercapacitors. Zhou and his colleges successfully prepared 3D PCN@V<sub>2</sub>O<sub>5</sub> electrodes (Zhou et al., 2020e). In the electrochemical performance test, the PCN@V<sub>2</sub>O<sub>5</sub> electrode showed a high specific capacity with 457 Fg<sup>-1</sup> at 0.5 Ag<sup>-1</sup> and outstanding cycling performance which could perpetuate good performance after 500 cycles. Moreover, 3D CNBMs are considered to be promising candidate materials for electrochemical sensors by reason of the chemical stability, electrical conductivity, considerable specific surface area, and enormous active sites. Wang and co-authors prepared a glass carbon electrode based on multi-walled carbon nanotubes / g-C<sub>3</sub>N<sub>4</sub> nanosheets (MWNTs / g-C<sub>3</sub>N<sub>4</sub>) (Wang et al., 2016a). This porous and loose structure made the g-C<sub>3</sub>N<sub>4</sub> / MWNTs / GCE show high sensitivity to dopamine, uric acid, and tryptophan. What's more, the sensor had been successfully used to measure these compounds in human serum and urine samples.

## 5. Conclusions and Perspectives

In this review, the synthetic methods of 3D CNBMs and 3D CNBMs composites have been discussed in detail. The synthesis method of 3D CNBMs mainly includes hard template method, soft template method, and self-template method. Some methods like thermal polymerization, freeze-drying, heat-cooling, and hydrothermal / solvent-thermal have been also explored for synthesizing 3D CNBMs composites. Furthermore, 3D CNBMs have shown extensive applications in photocatalysis, electrochemistry, and photochemistry owing to their special electronic structure and band structure.

Compared with bulk g-C<sub>3</sub>N<sub>4</sub>, 3D CNBMs have more stable frameworks. However, there are still some problems and challenges needed to be considered:

(1) Although there are more and more studies on 3D CNBMs, most of them are based on the modification of 2D CNBMs. The 3D CNBMs are mostly obtained by means of doping modification and constructing heterogeneous composites. However, the modification studies based on 3D CNBMs are relatively few, and future research can be developed in this direction.

(2) Most studies on the performance of 3D CNBMs photocatalyst focus on the improvement of catalytic performance through modifications. However, there is a lack of research on the mechanism of how these modification methods can improve the catalytic activities.

(3) The porous structure of 3D CNBMs can effectively adsorb the reactant and provide the active sites, but the adsorption and desorption processes have been rarely studied. In future studies, it can be explored from the perspective of thermodynamics and kinetics.

(4) Despite the increasing studies on 3D CNBMs, there are relatively fewer reports on 3D CNBMs compared with g-C<sub>3</sub>N<sub>4</sub>. These studies mostly focus on applications in photocatalysis, and there are few studies in electrocatalysis and photo-electrocatalysis. Subsequent research can be conducted in diverse aspects to fully realize the value of 3D CNBMs.

**Acknowledgements.** This study was financially supported by the Program for the National Natural Science Foundation of China (U20A20323, 51879101), the National Program for Support of Top-Notch Young Professionals of China (2014), the Fundamental Research Funds for the Central Universities, Hunan Provincial Science and Technology Plan Project (No.2016RS3026, 2017SK2243, 2018SK20410), the Fundamental Research Funds for the Central Universities (531119200086, 531118010114, 531107050978, 541109060031, 531118010574), the Program for Changjiang Scholars and Innovative Research Team in University (IRT-13R17), and the Three Gorges Follow-up Research Project (2017HXXY-05).

## References

- Ai, M.H., Zhang, J.W., Gao, R.J., Pan, L., Zhang, X.W. and Zou, J.J. (2019). MnOx-decorated 3D porous C<sub>3</sub>N<sub>4</sub> with internal donoracceptor motifs for efficient photocatalytic hydrogen production. *Appl. Catal. B.*, 256, 117805. <http://doi.org/10.1016/j.apcatb.2019.117805>
- Bai, W.D., Yang, X.Z., Du, X.L., Qian, Z.Q., Zhang, Y., Liu, L. and Yao, J.M. (2020). Robust and recyclable macroscopic g-C<sub>3</sub>N<sub>4</sub>/cellulose hybrid photocatalysts with enhanced visible light photocatalytic activity. *Appl. Surf. Sci.*, 504, 144179. <http://doi.org/10.1016/j.apsusc.2019.144179>
- Cao, J. and Zhou, Y. (2017). Excited state relaxation processes of H<sub>2</sub>-evolving Ru-Pd supramolecular photocatalysts containing a linear or non-linear bridge: a DFT and TDDFT study. *Phys. Chem. Chem. Phys.*, 19(18), 11529-11539. <http://doi.org/10.1039/c6cp07857e>
- Chen, W., Liu, M., Li, X.Y. and Mao, L.Q. (2020). Synthesis of 3D mesoporous g-C<sub>3</sub>N<sub>4</sub> for efficient overall water splitting under a Z-scheme photocatalytic system. *Appl. Surf. Sci.*, 512, 145782. <http://doi.org/10.1016/j.apsusc.2020.145782>
- Chen, X.J., Shi, R., Chen, Q., Zhang, Z.J., Jiang, W.J., Zhu, Y.F. and Zhang, T.R. (2019). Three-dimensional porous g-C<sub>3</sub>N<sub>4</sub> for highly efficient photocatalytic overall water splitting. *Nano Energy*, 59, 644-650. <http://doi.org/10.1016/j.nanoen.2019.03.010>
- Cheng, L., Xiang, Q.J., Liao, Y.L. and Zhang, H.W. (2018). CdS-Based photocatalysts. *Energy Environ. Sci.*, 11(6), 1362-1391. <http://doi.org/10.1039/c7ee03640j>
- Cheng, M., Liu, Y., Huang, D.L., Lai, C., Zeng, G.M., Huang, J.H., Liu, Z.F., Zhang, C., Zhou, C.Y. and Qin, L. (2019). Prussian blue analogue derived magnetic Cu-Fe oxide as a recyclable photo-Fenton catalyst for the efficient removal of sulfamethazine at near neutral pH values. *Chem. Eng. J.*, 362, 865-876. <http://doi.org/10.1016/j.cej.2019.01.101>

- Di Mauro, A., Fragalà, M.E., Privitera, V. and Impellizzeri, G. (2017). ZnO for application in photocatalysis: From thin films to nanostructures. *Mater. Sci. Semicond. Process.*, 69, 44-51. <http://doi.org/10.1016/j.mssp.2017.03.029>
- Di, T.M., Zhu, B.C., Cheng, B., Yu, J.G. and Xu, J.S. (2017). A direct Z-scheme g-C<sub>3</sub>N<sub>4</sub>/SnS<sub>2</sub> photocatalyst with superior visible-light CO<sub>2</sub> reduction performance. *J Catal.*, 352, 532-541. <http://doi.org/10.1016/j.jcat.2017.06.006>
- Dong, F., Zhao, Z.W., Xiong, T., Ni, Z.L., Zhang, W.D., Sun, Y.J. and Ho, W. (2013). In situ construction of g-C<sub>3</sub>N<sub>4</sub>/g-C<sub>3</sub>N<sub>4</sub> metal-free heterojunction for enhanced visible-light photocatalysis. *ACS Appl. Mater. Interfaces*, 5(21), 11392-11401. <http://doi.org/10.1021/am403653a>
- Du, J.Y., Fan, Y.F., Gan, X.R., Dang, X.M. and Zhao, H.M. (2020). Three-dimension branched crystalline carbon nitride: A high efficiency photoelectrochemical sensor of trace Cu<sup>2+</sup> detection. *Electrochim.*, 330, 135336. <http://doi.org/10.1016/j.electacta.2019.135336>
- Duan, M., Jiang, L., Zeng, G., Wang, D., Tang, W., Liang, J., Wang, H., He, D., Liu, Z. and Tang, L. (2020). Bimetallic nanoparticles/metal-organic frameworks: Synthesis, applications and challenges. *Appl. Mater. Today.*, 19, 100564. <http://doi.org/10.1016/j.apmt.2020.100564>
- Fu, J.W., Xu, Q.L., Low, J.X., Jiang, C.J. and Yu, J.G. (2019). Ultrathin 2D/2D WO<sub>3</sub>/g-C<sub>3</sub>N<sub>4</sub> step-scheme H<sub>2</sub>-production photocatalyst. *Appl. Catal. B.*, 243, 556-565. <http://doi.org/10.1016/j.apcatb.2018.11.011>
- Fu, J.W., Zhu, B.C., Jiang, C.J., Cheng, B., You, W. and Yu, J.G. (2017). Hierarchical Porous O-Doped g-C<sub>3</sub>N<sub>4</sub> with Enhanced Photocatalytic CO<sub>2</sub> Reduction Activity. *Small*, 13(15), 1603938. <http://doi.org/10.1002/smll.201603938>
- Ge, M., Li, Y.F., Liu, L., Zhou, Z. and Chen, W. (2011). Bi<sub>2</sub>O<sub>3</sub>-Bi<sub>2</sub>WO<sub>6</sub> Composite Microspheres: Hydrothermal Synthesis and Photocatalytic Performances. *J. Phys. Chem. C.*, 115(13), 5220-5225. <http://doi.org/10.1021/jp108414e>
- Golestanbagh, M., Parvini, M. and Pendashteh, A. (2018). Preparation, Characterization and Photocatalytic Properties of Visible-Light-Driven CuO/SnO<sub>2</sub>/TiO<sub>2</sub> Photocatalyst. *Catal. Letters*, 148(7), 2162-2178. <http://doi.org/10.1007/s10562-018-2385-5>
- Gu, J.Y., Liu, M.G., Xun, S.H., He, M.Q., Wu, L.L., Zhu, L.H., Wu, X.Y., Zhu, W.S. and Li, H.M. (2020). Lipophilic decavanadate supported by three-dimensional porous carbon nitride catalyst for aerobic oxidative desulfurization. *Mol. Catal.*, 483, 110709. <http://doi.org/10.1016/j.mcat.2019.110709>
- Gu, W.L., Hu, L.Y., Li, J. and Wang, E. (2016). Hybrid of g-C<sub>3</sub>N<sub>4</sub> Assisted Metal-Organic Frameworks and Their Derived High-Efficiency Oxygen Reduction Electrocatalyst in the Whole pH Range. *ACS Appl. Mater. Interfaces*, 8(51), 35281-35288. <http://doi.org/10.1021/acsami.6b12031>
- Gupta, B., Gupta, A.K., Ghosal, P.S. and Tiwary, C.S. (2020). Photo-induced degradation of bio-toxic Ciprofloxacin using the porous 3D hybrid architecture of an atomically thin sulfur-doped g-C<sub>3</sub>N<sub>4</sub>/ZnO nanosheet. *Environ. Res.*, 183, 109154. <http://doi.org/10.1016/j.envres.2020.109154>
- He, B., Liu, R., Ren, J.B., Tang, C.J., Zhong, Y.J. and Hu, Y. (2017). One-Step Solvothermal Synthesis of Petalous Carbon-Coated Cu<sup>+</sup>-Doped CdS Nanocomposites with Enhanced Photocatalytic Hydrogen Production. *Langmuir*, 33(27), 6719-6726. <http://doi.org/10.1021/acs.langmuir.7b01450>
- He, L., Li, Y.P., Zhu, F.P., Sun, X.M., Herrmann, H., Schaefer, T., Zhang, Q.Z. and Wang, S.G. (2020). Insight into the Mechanism of the OH-Induced Reaction of Ketoprofen: A Combined DFT Simulation and Experimental Study. *J. Environ. Inform.*, 35(2), 128-137. <http://doi.org/10.3808/jei.201900408>
- He, R.A., Zhou, J.Q., Fu, H.Q., Zhang, S.Y. and Jiang, C.J. (2018). Room-temperature in situ fabrication of Bi<sub>2</sub>O<sub>3</sub>/g-C<sub>3</sub>N<sub>4</sub> direct Z-scheme photocatalyst with enhanced photocatalytic activity. *Appl. Surf. Sci.*, 430, 273-282. <http://doi.org/10.1016/j.apsusc.2017.07.191>
- He, Y.M., Zhang, L.H., Teng, B.T. and Fan, M.H. (2015). New Application of Z-Scheme Ag<sub>3</sub>PO<sub>4</sub>/g-C<sub>3</sub>N<sub>4</sub> Composite in Converting CO<sub>2</sub> to Fuel. *Environ. Sci. Technol.*, 49(1), 649-656. <http://doi.org/10.1021/es5046309>
- Hu, X.L., Zhang, W.J., Yong, Y.W., Xu, Y., Wang, X.H. and Yao, X.X. (2020). One-step synthesis of iodine-doped g-C<sub>3</sub>N<sub>4</sub> with enhanced photocatalytic nitrogen fixation performance. *Appl. Surf. Sci.*, 510, 145413. <http://doi.org/10.1016/j.apsusc.2020.145413>
- Huang, G.W., Liu, H., Li, X. and Ma, M. (2019). Exploring Drivers of Nitrate Contamination of Drinking Water in an Arid Region of China. *J. Environ. Inform.*, 33(2), 105-112. <http://doi.org/10.3808/jei.201900409>
- Huang, J., Huang, G., An, C., Xin, X., Chen, X., Zhao, Y., Feng, R. and Xiong, W. (2020a). Exploring the use of ceramic disk filter coated with Ag/ZnO nanocomposites as an innovative approach for removing Escherichia coli from household drinking water. *Chemosphere*, 245, 125545. <http://doi.org/10.1016/j.chemosphere.2019.125545>
- Huang, Z.Z., Zeng, Z.T., Song, Z.X., Chen, A.W., Zeng, G.M., Xiao, R., He, K., Yuan, L., Li, H. and Chen, G.Q. (2020b). Antimicrobial efficacy and mechanisms of silver nanoparticles against Phanerochaete chrysosporium in the presence of common electrolytes and humic acid. *J. Hazard. Mater.*, 383, 121153. <https://doi.org/10.1016/j.jhazmat.2019.121153>
- Huo, R., Yang, X.L., Yang, J.Y., Yang, S.Y. and Xu, Y.H. (2018). Self-assembly synthesis of BiVO<sub>4</sub>/Polydopamine/g-C<sub>3</sub>N<sub>4</sub> with enhanced visible light photocatalytic performance. *Mater. Res. Bull.*, 98, 225-230. <http://doi.org/10.1016/j.materresbull.2017.10.016>
- Ji, L., Huang, G.H., Niu, D.X., Cai, Y.P. and Yin, J.G. (2020). A Stochastic Optimization Model for Carbon-Emission Reduction Investment and Sustainable Energy Planning under Cost-Risk Control. *J. Environ. Inform.*, 36(2), 107-118. <http://doi.org/10.3808/jei.202000428>
- Jiang, Z., Yang, F., Yang, G.D., Kong, L., Jones, M.O., Xiao, T. and Edwards, P.P. (2010). The hydrothermal synthesis of BiOBr flakes for visible-light-responsive photocatalytic degradation of methyl orange. *J. Photochem. Photobiol. A.*, 212(1), 8-13. <http://doi.org/10.1016/j.jphotochem.2010.03.004>
- Khan, A., Alam, U., Raza, W., Bahnemann, D. and Munee, M. (2018). One-pot, self-assembled hydrothermal synthesis of 3D flower-like CuS/g-C<sub>3</sub>N<sub>4</sub> composite with enhanced photocatalytic activity under visible-light irradiation. *J. Phys. Chem. Solids*, 115, 59-68. <http://doi.org/10.1016/j.jpcs.2017.10.032>
- Kim, C., Cho, K.M., Park, K., Kim, K.H., Gereige, I. and Jung, H. (2020). Ternary Hybrid Aerogels of g-C<sub>3</sub>N<sub>4</sub>/ $\alpha$ -Fe<sub>2</sub>O<sub>3</sub> on a 3D Graphene Network: An Efficient and Recyclable Z-Scheme Photocatalyst. *Chem-PlusChem*, 85(1), 169-175. <http://doi.org/10.1002/cplu.201900688>
- Koci, K., Van, H.D., Edelmannova, M., Reli, M. and Wu, J.C.S. (2020). Photocatalytic reduction of CO<sub>2</sub> using Pt/C<sub>3</sub>N<sub>4</sub> photocatalysts. *Appl. Surf. Sci.*, 503, 144426. <http://doi.org/10.1016/j.apsusc.2019.144426>
- Kudo, A. and Miseki, Y. (2009). Heterogeneous photocatalyst materials for water splitting. *Chem. Soc. Rev.*, 38(1), 253-278. <http://doi.org/10.1039/B800489G>
- Li, B.Y., Cao, Z.H., Wang, S.X., Wei, Q. and Shen, Z.R. (2018a). BiVO<sub>4</sub> quantum dot-decorated BiPO<sub>4</sub> nanorods 0D/1D heterojunction for enhanced visible-light-driven photocatalysis. *Dalton Trans.*, 47 (30), 10288-10298. <http://doi.org/10.1039/c8dt02402b>
- Li, C.Q., Sun, Z.M., Zhang, W.Z., Yu, C.H. and Zheng, S.L. (2018b). Highly efficient g-C<sub>3</sub>N<sub>4</sub>/TiO<sub>2</sub>/kaolinite composite with novel three-dimensional structure and enhanced visible light responding ability towards ciprofloxacin and S. aureus. *Appl. Catal. B.*, 220, 272-282. <http://doi.org/10.1016/j.apcatb.2017.08.044>
- Li, X., Xiong, J., Gao, X.m., Huang, J.t., Feng, Z.j., Chen, Z. and Zhu, Y.f. (2019). Recent advances in 3D g-C<sub>3</sub>N<sub>4</sub> composite photocatalysts for photocatalytic water splitting, degradation of pollutants and CO<sub>2</sub> reduction. *J. Alloys Compd.*, 802, 196-209. <http://doi.org/10.1016/j.jallcom.2019.06.185>

- Li, X.B., Zhang, H.S., Luo, J.M., Feng, Z.J. and Huang, J.T. (2017). Hydrothermal synthesized novel nanoporous g-C<sub>3</sub>N<sub>4</sub>/MnTiO<sub>3</sub> heterojunction with direct Z-scheme mechanism. *Electrochim.*, 258, 998-1007. <http://doi.org/10.1016/j.electacta.2017.11.151>
- Li, X.G., Bi, W.T., Zhang, L., Tao, S., Chu, W.S., Zhang, Q., Luo, Y., Wu, C.Z. and Xie, Y. (2016). Single-Atom Pt as Co-Catalyst for Enhanced Photocatalytic H<sub>2</sub> Evolution. *Adv. Mater.*, 28(12), 2427-2431. <http://doi.org/10.1016/j.cej.2019.123091>
- Li, X.P., Zeng, Z.T., Zeng, G.M., Wang, D.B., Xiao, R., Wang, Y.R., Zhou, C.Y., Yi, H., Ye, S.J., Yang, Y. and Xiong, W.P. (2020). A "bottle-around-ship" like method synthesized yolk-shell Ag<sub>3</sub>PO<sub>4</sub> @MIL-53(Fe) Z-scheme photocatalysts for enhanced tetracycline removal. *J. Colloid Interface Sci.*, 561, 501-511. <http://doi.org/10.1016/j.jcis.2019.11.025>
- Li, Y.P., Gao, J.Y., Zhang, F., Qian, Q.Z., Liu, Y. and Zhang, G.Q. (2018c). Hierarchical 3D macrosheets composed of interconnected in situ cobalt catalyzed nitrogen doped carbon nanotubes as superior bifunctional oxygen electrocatalysts for rechargeable Zn-air batteries. *J. Mater. Chem. A.*, 6(32), 15523-15529. <http://doi.org/10.1039/c8ta06057f>
- Liu, H.Y., Liang, C., Niu, C.G., Huang, D.W., Du, Y.B., Guo, H., Zhang, L., Yang, Y.Y. and Zeng, G.M. (2019). Facile assembly of g-C<sub>3</sub>N<sub>4</sub>/Ag<sub>2</sub>CO<sub>3</sub>/graphene oxide with a novel dual Z-scheme system for enhanced photocatalytic pollutant degradation. *Appl. Surf. Sci.*, 475, 421-434. <http://doi.org/10.1016/j.apsusc.2019.01.018>
- Liu, J.H., Zhang, Y.W., Lu, L.H., Wu, G. and Chen, W. (2012). Self-regenerated solar-driven photocatalytic water-splitting by urea derived graphitic carbon nitride with platinum nanoparticles. *Chem. Commun.*, 48(70), 8826-8828. <http://doi.org/10.1039/c2cc33644h>
- Liu, Q. and Zhang, J.Y. (2013). Graphene Supported Co-g-C<sub>3</sub>N<sub>4</sub> as a Novel Metal-Macrocyclic Electrocatalyst for the Oxygen Reduction Reaction in Fuel Cells. *Langmuir*, 29(11), 3821-3828. <http://doi.org/10.1021/la400003h>
- Liu, W., Su, C., Liu, D. and Wen, F. (2021). Three-dimensional ordered macroporous materials with g-C<sub>3</sub>N<sub>4</sub> and TiO<sub>2</sub> as pore walls for efficient photocatalytic hydrogen evolution. *Colloids Surf. A Physico-chem. Eng. Asp.*, 609, 125681. <http://doi.org/10.1016/j.colsurfa.2020.125681>
- Liu, X.M., Liu, Y., Zhang, W.K., Zhong, Q.Y. and Ma, X.Y. (2020). In situ self-assembly of 3D hierarchical 2D/2D CdS/g-C<sub>3</sub>N<sub>4</sub> heterojunction with excellent photocatalytic performance. *Mater. Sci. Semicond. Process.*, 105, 104734. <http://doi.org/10.1016/j.mssp.2019.104734>
- Lu, X.L., Xu, K., Chen, P.Z., Jia, K.C., Liu, S. and Wu, C.Z. (2014). Facile one step method realizing scalable production of g-C<sub>3</sub>N<sub>4</sub> nanosheets and study of their photocatalytic H<sub>2</sub> evolution activity. *J. Mater. Chem.*, 2(44), 18924-18928. <http://doi.org/10.1039/C4TA04487H>
- Luo, B., Song, R., Geng, J., Jing, D. and Zhang, Y. (2018). Facile preparation with high yield of a 3D porous graphitic carbon nitride for dramatically enhanced photocatalytic H<sub>2</sub> evolution under visible light. *Appl. Catal. B.*, 238, 294-301. <http://doi.org/10.1016/j.apcatb.2018.07.039>
- Luo, S.H., Zeng, Z.T., Zeng, G.M., Liu, Z.F., Xiao, R., Xu, P., Wang, H., Huang, D.L., Liu, Y., Shao, B.B., Liang, Q.H., Wang, D.B., He, Q.Y., Qin, L. and Fu, Y.K. (2020). Recent advances in conjugated microporous polymers for photocatalysis: designs, applications, and prospects. *J. Mater. Chem. A.*, 8(14), 6434-6470. <http://doi.org/10.1039/d0ta01102a>
- Lv, S.Z., Zhang, K.Y., Zhou, Q. and Tang, D.P. (2020). Plasmonic enhanced photoelectrochemical aptasensor with D-A F8BT/g-C<sub>3</sub>N<sub>4</sub> heterojunction and AuNPs on a 3D-printed device. *Sens. Actuators B Chem.*, 310, 127874. <http://doi.org/10.1016/j.snb.2020.127874>
- Mohamed, M.A., M. Zain, M.F., Jeffery Minggu, L., Kassim, M.B., Saidina Amin, N.A., W. Salleh, W.N., Salehmin, M.N.I., Md Nasir, M.F. and Mohd Hir, Z.A. (2018). Constructing bio-templated 3D porous microtubular C-doped g-C<sub>3</sub>N<sub>4</sub> with tunable band structure and enhanced charge carrier separation. *Appl. Catal. B*, 236, 265-279. <http://doi.org/10.1016/j.apcatb.2018.05.037>
- Nakamura, I., Negishi, N., Kutsuna, S., Ihara, T., Sugihara, S. and Takeuchi, K. (2000). Role of oxygen vacancy in the plasma-treated TiO<sub>2</sub> photocatalyst with visible light activity for NO removal. *J. Mol. Catal. A Chem.*, 161(1), 205-212. [http://doi.org/10.1016/S1381-1169\(00\)00362-9](http://doi.org/10.1016/S1381-1169(00)00362-9)
- Ong, W., Tan, L., Ng, Y.H., Yong, S.T. and Chai, S. (2016). Graphitic Carbon Nitride (g-C<sub>3</sub>N<sub>4</sub>)-Based Photocatalysts for Artificial Photosynthesis and Environmental Remediation: Are We a Step Closer to Achieving Sustainability? *Chem. Rev.*, 116(12), 7159-7329. <http://doi.org/10.1021/acs.chemrev.6b00075>
- Qi, H.J., Ji, X.D., Shi, C., Ma, R.X., Huang, Z.H., Guo, M.H., Li, J. and Guo, Z.H. (2019). Bio-templated 3D porous graphitic carbon nitride hybrid aerogel with enhanced charge carrier separation for efficient removal of hazardous organic pollutants. *J. Colloid Interface Sci.*, 556, 366-375. <http://doi.org/10.1016/j.jcis.2019.08.072>
- Qian, X.Y., Meng, X.Y., Sun, J.W., Jiang, L.L., Wang, Y.N., Zhang, J.L., Hu, X.M., Shalom, M. and Zhu, J.W. (2019). Salt-Assisted Synthesis of 3D Porous g-C<sub>3</sub>N<sub>4</sub> as a Bifunctional Photo- and Electrocatalyst. *ACS Appl. Mater. Interfaces*, 11(30), 27226-27232. <http://doi.org/10.1021/acsami.9b08651>
- Qin, F., Peng, Y., Song, G., Fang, Q., Wang, R., Zhang, C., Zeng, G., Huang, D., Lai, C., Zhou, Y., Tan, X., Cheng, M. and Liu, S. (2020). Degradation of sulfamethazine by biochar-supported bimetallic oxide/persulfate system in natural water: Performance and reaction mechanism. *J. Hazard. Mater.*, 398, 122816. <http://doi.org/10.1016/j.jhazmat.2020.122816>
- Qin, Y., Li, J., Yuan, J., Kong, Y., Tao, Y.X., Lin, F.R. and Li, S. (2014). Hollow mesoporous carbon nitride nanosphere/three-dimensional graphene composite as high efficient electrocatalyst for oxygen reduction reaction. *J. Power Sources*, 272, 696-702. <http://doi.org/10.1016/j.jpowsour.2014.09.017>
- Sakthivel, S., Shankar, M.V., Palanichamy, M., Arabindoo, B., Bahnemann, D.W. and Murugesan, V. (2004). Enhancement of photocatalytic activity by metal deposition: characterisation and photonic efficiency of Pt, Au and Pd deposited on TiO<sub>2</sub> catalyst. *Water Res.*, 38(13), 3001-3008. <http://doi.org/10.1016/j.watres.2004.04.046>
- Sánchez-Rodríguez, D., Méndez Medrano, M.G., Remita, H. and Escobar-Barrios, V. (2018). Photocatalytic properties of BiOCl-TiO<sub>2</sub> composites for phenol photodegradation. *J. Environ. Chem. Eng.*, 6(2), 1601-1612. <http://doi.org/10.1016/j.jece.2018.01.061>
- Scuderi, V., Amiari, G., Boninelli, S., Scalese, S., Miritello, M., Sberna, P.M., Impellizzeri, G. and Privitera, V. (2016). Photocatalytic activity of CuO and Cu<sub>2</sub>O nanowires. *Mater. Sci. Semicond. Proces.*, 42, 89-93. <http://doi.org/10.1016/j.mssp.2015.08.008>
- Shakeel, M., Arif, M., Yasin, G., Li, B. and Khan, H.D. (2019). Layered by layered Ni-Mn-LDH/g-C<sub>3</sub>N<sub>4</sub> nanohybrid for multi-purpose photo/electrocatalysis: Morphology controlled strategy for effective charge carriers separation. *Appl. Catal. B*, 242, 485-498. <http://doi.org/10.1016/j.apcatb.2018.10.005>
- Shen, B., Hong, Z.h., Chen, Y.l., Lin, B.Z. and Gao, B.f. (2014). Template-free synthesis of a novel porous g-C<sub>3</sub>N<sub>4</sub> with 3D hierarchical structure for enhanced photocatalytic H<sub>2</sub> evolution. *Mater. Lett.*, 118, 208-211. <http://doi.org/10.1016/j.matlet.2013.12.070>
- Sheng, Y.Q., Wei, Z., Miao, H., Yao, W.Q., Li, H.Q. and Zhu, Y.F. (2019). Enhanced organic pollutant photodegradation via adsorption/photocatalysis synergy using a 3D g-C<sub>3</sub>N<sub>4</sub>/TiO<sub>2</sub> free-separation photocatalyst. *Chem. Eng. J.*, 370, 287-294. <http://doi.org/10.1016/j.cej.2019.03.197>
- Shi, Q.Q., Ping, G.C., Wang, X.J., Xu, H., Li, J.M., Cui, J.Q., Abroshan, H., Ding, H.J. and Li, G. (2019). CuO/TiO<sub>2</sub> heterojunction composites: an efficient photocatalyst for selective oxidation of methanol to methyl formate. *J. Mater. Chem. A*, 7(5), 2253-2260. <http://doi.org/10.1039/c8ta09439j>

- Si, Y., Zhang, X.X., Liang, T.T., Xu, X., Qiu, L.F., Li, P. and Duo, S.W. (2020). Facile in-situ synthesis of 2D/3D g-C<sub>3</sub>N<sub>4</sub>/Cu<sub>2</sub>O heterojunction for high-performance photocatalytic dye degradation. *Mater. Res. Express*, 7(1), 015524. <http://doi.org/10.1088/2053-1591/ab6893>
- Silva, C.u.G., Jua'rez, R., Marino, T., Molinari, R. and Garc'a, H. (2011). Influence of Excitation Wavelength (UV or Visible Light) on the photocatalytic activity of titania containing gold nanoparticles for the generation of hydrogen or oxygen from water. *J. Am. Chem. Soc.*, 133(3), 595-602. <http://doi.org/10.1021/ja1086358>
- Sun, M., Yan, Q., Yan, T., Li, M.M., Wei, D., Wang, Z.P., Wei, Q. and Du, B. (2014). Facile fabrication of 3D flower-like heterostructured g-C<sub>3</sub>N<sub>4</sub>/SnS<sub>2</sub> composite with efficient photocatalytic activity under visible light. *Rsc Adv.*, 4(59), 31019-31027. <http://doi.org/10.1039/c4ra03843f>
- Sun, Z.M., Fang, W., Zhao, L. and Wang, H.L. (2020). 3D porous Cu-NPs/g-C<sub>3</sub>N<sub>4</sub> foam with excellent CO<sub>2</sub> adsorption and Schottky junction effect for photocatalytic CO<sub>2</sub> reduction. *Appl. Surf. Sci.*, 504, 144347. <http://doi.org/10.1016/j.apsusc.2019.144347>
- Tan, L., Yu, C.F., Wang, M., Zhang, S.Y., Sun, J.Y., Dong, S.Y. and Sun, J.H. (2019). Synergistic effect of adsorption and photo-catalysis of 3D g-C<sub>3</sub>N<sub>4</sub>-agar hybrid aerogels. *Appl. Surf. Sci.*, 467-468, 286-292. <http://doi.org/10.1016/j.apsusc.2018.10.067>
- Tang, J.Y., Kong, X.Y., Ng, B.J., Chew, Y.H., Mohamed, A.R. and Chai, S.P. (2019). Midgap-state-mediated two-step photoexcitation in nitrogen defect-modified g-C<sub>3</sub>N<sub>4</sub> atomic layers for superior photocatalytic CO<sub>2</sub> reduction. *Catal. Sci. Technol.*, 9(9), 2335-2343. <http://doi.org/10.1039/c9cy00449a>
- Tian, J.Q., Ning, R., Liu, Q., Asiri, A.M., Alyoubi, A.O. and Sun, X.P. (2014). Three-Dimensional Porous Supramolecular Architecture from Ultrathin g-C<sub>3</sub>N<sub>4</sub> Nanosheets and Reduced Graphene Oxide: Solution Self-Assembly Construction and Application as a Highly Efficient Metal-Free Electrocatalyst for Oxygen Reduction Reaction. *ACS Appl. Mater. Interfaces*, 6(2), 1011-1017. <http://doi.org/10.1021/am404536w>
- Tomer, V.K., Thangaraj, N., Gahlot, S. and Kailasam, K. (2016). Cubic mesoporous Ag@CN: a high performance humidity sensor. *Nanoscale*, 8(47), 19794-19803. <http://doi.org/10.1039/c6nr08039a>
- Wan, W.C., Yu, S., Dong, F., Zhang, Q. and Zhou, Y. (2016). Efficient C<sub>3</sub>N<sub>4</sub>/graphene oxide macroscopic aerogel visible-light photocatalyst. *J. Mater. Chem. A*, 4(20), 7823-7829. <http://doi.org/10.1039/c6ta01804a>
- Wang, C., Li, J., Luo, X.Y., Hui, J.M., Liu, X., Tan, J. and Zhao, X. (2016a). Graphitic carbon nitride nanosheets modified multi-walled carbon nanotubes as 3D high efficient sensor for simultaneous determination of dopamine, uric acid and tryptophan. *J. Electroanal. Chem.*, 780, 147-152. <http://doi.org/10.1016/j.jelechem.2016.09.004>
- Wang, D.D., Li, J., Xu, Z.F., Zhu, Y.R., Chen, G.X. and Cui, Z. (2019a). Synthesis of g-C<sub>3</sub>N<sub>4</sub>/NiO p-n heterojunction materials with ball-flower morphology and enhanced photocatalytic performance for the removal of tetracycline and Cr<sup>6+</sup>. *J. Mater. Sci.*, 54(17), 11417-11434. <http://doi.org/10.1007/s10853-019-03692-5>
- Wang, H., Wang, H.Q., Wang, Z.W., Tang, L., Zeng, G.M., Xu, P., Chen, M., Xiong, T., Zhou, C.Y., Li, X.Y., Huang, D.L., Zhu, Y., Wang, Z.X. and Tang, J.W. (2020a). Covalent organic framework photocatalysts: structures and applications. *Chem. Soc. Rev.*, 49 (12), 4135-4165. <http://doi.org/10.1039/d0cs00278j>
- Wang, H.q., Zhang, X.D., Xie, J.F., Zhang, J.J., Ma, P., Pan, B.C. and Xie, Y. (2015a). Structural distortion in graphitic-C<sub>3</sub>N<sub>4</sub> realizing an efficient photoreactivity. *Nanoscale*, 7(12), 5152-5156. <http://doi.org/10.1039/c4nr07645a>
- Wang, J.X., Huang, J., Xie, H.L. and Qu, A.L. (2014). Synthesis of g-C<sub>3</sub>N<sub>4</sub>/TiO<sub>2</sub> with enhanced photocatalytic activity for H<sub>2</sub> evolution by a simple method. *Int. J. Hydrol. Energy*, 39(12), 6354-6363. <http://doi.org/10.1016/j.ijhydene.2014.02.020>
- Wang, K., Li, Q., Liu, B.S., Cheng, B., Ho, W.K. and Yu, J.G. (2015b). Sulfur-doped g-C<sub>3</sub>N<sub>4</sub> with enhanced photocatalytic CO<sub>2</sub>- reduction performance. *Appl. Catal. B*, 176, 44-52. <http://doi.org/10.1016/j.apcatb.2015.03.045>
- Wang, L., Liu, S., Wang, Z., Zhou, Y., Qin, Y. and Wang, Z.L. (2016b). Piezotronic Effect Enhanced Photocatalysis in Strained Anisotropic ZnO/TiO<sub>2</sub> Nanoplatelets via Thermal Stress. *ACS Nano*, 10(2), 2636-2643. <http://doi.org/10.1021/acsnano.5b07678>
- Wang, W.J., Zeng, Z.T., Zeng, G.M., Zhang, C., Xiao, R., Zhou, C.Y., Xiong, W.P., Yang, Y., Lei, L. and Liu, Y. (2019b). Sulfur doped carbon quantum dots loaded hollow tubular g-C<sub>3</sub>N<sub>4</sub> as novel photocatalyst for destruction of Escherichia coli and tetracycline degradation under visible light. *Chem. Eng. J.*, 378, 122132. <http://doi.org/10.1016/j.cej.2019.122132>
- Wang, W.J., Niu, Q.Y., Zeng, G.M., Zhang, C., Huang, D.L., Shao, B.B., Zhou, C.Y., Yang, Y., Liu, Y.X., Guo, H., Xiong, W.P., Lei, L., Liu, S.Y., Yi, H., Chen, S. and Tang, X. (2020b). 1D porous tubular g-C<sub>3</sub>N<sub>4</sub> capture black phosphorus quantum dots as 1D/0D metal-free photocatalysts for oxytetracycline hydrochloride degradation and hexavalent chromium reduction. *Appl. Catal. B*, 273, 119051. <http://doi.org/https://doi.org/10.1016/j.apcatb.2020.119051>
- Wang, W.J., Zhou, C.Y., Yang, Y., Zeng, G.M., Zhang, C., Zhou, Y., Yang, J.N., Huang, D.L., Wang, H., Xiong, W.P., Li, X.P., Fu, Y.K., Wang, Z.W., He, Q.Y., Jia, M.Y. and Luo, H.Z. (2021a). Carbon nitride based photocatalysts for solar photocatalytic disinfection, can we go further? *Chem. Eng. J.*, 404, 126540. <http://doi.org/10.1016/j.cej.2020.126540>
- Wang, X., Li, Q., Gan, L., Ji, X., Chen, F., Peng, X. and Zhang, R. (2021b). 3D macropore carbon-vacancy g-C<sub>3</sub>N<sub>4</sub> constructed using polymethylmethacrylate spheres for enhanced photocatalytic H<sub>2</sub> evolution and CO<sub>2</sub> reduction. *J. Energy Chem.*, 53, 139-146. <http://doi.org/10.1016/j.jechem.2020.05.001>
- Wang, X., Maeda, K., Thomas, A., Takanabe, K., Xin, G., Carlsson, J.M., Domen, K. and Antonietti, M. (2009a). A metal-free polymeric photocatalyst for hydrogen production from water under visible light. *Nat. Mater.*, 8(1), 76-80. <http://doi.org/10.1038/nmat2317>
- Wang, X.C., Chen, X.F., Thomas, A., Fu, X.Z. and Antonietti, M. (2009b). Metal-containing carbon nitride compounds: a new functional organic-metal hybrid material. *Adv. Mater.*, 21(16), 1609-1612. <http://doi.org/10.1002/adma.200802627>
- Wang, Y.G., Xia, Q.N., Bai, X., Ge, Z.G., Yang, Q., Yin, C.C., Kang, S.F., Dong, M.D. and Li, X. (2018a). Carbothermal activation synthesis of 3D porous g-C<sub>3</sub>N<sub>4</sub>/carbon nanosheets composite with superior performance for CO<sub>2</sub> photoreduction. *Appl. Catal. B*, 239, 196-203. <http://doi.org/10.1016/j.apcatb.2018.08.018>
- Wang, Y.N., Zeng, Y.Q., Wan, S.P., Cai, W., Song, F.J., Zhang, S.L. and Zhong, Q. (2018b). In Situ Fabrication of 3D Octahedral g-C<sub>3</sub>N<sub>4</sub>/BiFeWO<sub>6</sub> Double-Heterojunction for Highly Selective CO<sub>2</sub> Photoreduction to CO Under Visible Light. *Chemcatchem.*, 10(20), 4578-4585. <http://doi.org/10.1002/cetc.201800959>
- Wang, Y.Q., Yin, X., Shen, H.B., Jiang, H., Yu, J.W., Zhang, Y.F., Li, D.W., Li, W.Z. and Li, J. (2018c). Co<sub>3</sub>O<sub>4</sub>@g-C<sub>3</sub>N<sub>4</sub> supported on N-doped graphene as effective electrocatalyst for oxygen reduction reaction. *Int. J. Hydrol. Energy*, 43(45), 20687-20695. <http://doi.org/10.1016/j.ijhydene.2018.09.140>
- Wang, Z.W., Wang, H., Zeng, Z.T., Zeng, G.M., Xu, P., Xiao, R., Huang, D.L., Chen, X.J., He, L.W. and Zhou, C.Y. (2020c). Metal-organic frameworks derived Bi<sub>2</sub>O<sub>3</sub>CO<sub>3</sub>/porous carbon nitride: A nano-sized Z-scheme systems with enhanced photocatalytic activity. *Appl. Catal. B*, 267, 118700. <http://doi.org/10.1016/j.apcatb.2020.118700>
- Wen, P., Sun, Y.H., Li, H., Liang, Z.Q., Wu, H.H., Zhang, J.C., Zeng, H.J., Geyer, S.M. and Jiang, L. (2020). A highly active three-dimensional Z-scheme ZnO/Au/g-C<sub>3</sub>N<sub>4</sub> photocathode for efficient photoelectrochemical water splitting. *Appl. Catal. B*, 263, 118180. <http://doi.org/10.1016/j.apcatb.2019.118180>
- Wu, H.P., Chen, J., Zeng, G.M., Xu, J.J., Sang, L.H., Liu, Q., Dai, J., Xiong, W.P., Yuan, Z., Wang, Y.Q. and Ye, S.J. (2020). Effects of Early Dry Season on Habitat Suitability for Migratory Birds in China's Two Largest Freshwater Lake Wetlands after the Impoundment of Three Gorges Dam. *J. Environ. Inform.*, 36(2), 82-92. <http://doi.org/10.1016/j.jenvinf.2020.01.002>

- doi.org/10.3808/jei.201900411
- Wu, X.Y., Li, S.M., Wang, B., Liu, J.H. and Yu, M. (2017). From biomass chitin to mesoporous nanosheets assembled loofa sponge-like N-doped carbon/g-C<sub>3</sub>N<sub>4</sub> 3D network architectures as ultralow-cost bifunctional oxygen catalysts. *Microporous Mesoporous Mater.*, 240, 216-226. <http://doi.org/10.1016/j.micromeso.2016.11.022>
- Xie, W.P., Yang, J.S., Yao, R.J. and Wang, X.P. (2020). Impact Study of Impoundment of the Three Gorges Reservoir on Salt-Water Dynamics and Soil Salinity in the Yangtze River Estuary. *J. Environ. Inform.*, 36(1), 11-23. <http://doi.org/10.3808/jei.202000432>
- Xie, Y.D., Kocaebe, D., Chen, C.Y. and Kocaebe, Y. (2016). Review of Research on Template Methods in Preparation of Nanomaterials. *J. Nanomater.*, 2016, 2302595. <http://doi.org/10.1155/2016/2302595>
- Xing, W., Zhang, M., Liang, J., Tang, W., Li, P., Luo, Y., Tang, N. and Guo, J. (2020). Facile synthesis of pinecone biomass-derived phosphorus-doping porous carbon electrodes for efficient electrochemical salt removal. *Sep. Purif. Technol.*, 251, 117357. <http://doi.org/10.1016/j.seppur.2020.117357>
- Xiong, Y., Chen, Y.P., Yang, N., Jin, C.D. and Sun, Q.F. (2019). WC1-x-Coupled 3D Porous Defective g-C<sub>3</sub>N<sub>4</sub> for Efficient Photocatalytic Overall Water Splitting. *Sol. RRL.*, 3(5), 1800341. <http://doi.org/10.1002/solr.201800341>
- Xue, W.J., Huang, D.L., Wen, X.J., Chen, S., Cheng, M., Deng, R., Li, B., Yang, Y. and Liu, X.G. (2020). Silver-based semiconductor Z-scheme photocatalytic systems for environmental purification. *J. Hazard. Mater.*, 390, 122128. <http://doi.org/10.1016/j.jhazmat.2020.122128>
- Yan, H.J. and Yang, H.X. (2011). TiO<sub>2</sub>-g-C<sub>3</sub>N<sub>4</sub> composite materials for photocatalytic H<sub>2</sub> evolution under visible light irradiation. *J. Alloys Compd.*, 509(4), L26-L29. <http://doi.org/10.1016/j.jallcom.2010.09.201>
- Yan, S.C., Li, Z.S. and Zou, Z.G. (2009). Photodegradation performance of g-C<sub>3</sub>N<sub>4</sub> fabricated by directly heating melamine. *Langmuir.*, 25(17), 10397-10401. <http://doi.org/10.1021/la900923z>
- Yan, X.D., Li, Y. and Xia, T. (2017a). Black Titanium Dioxide Nanomaterials in Photocatalysis. *Int. J. Photoenergy*, 2017, 1-16. <http://doi.org/10.1155/2017/8529851>
- Yan, X.R., Xu, R.P., Guo, J.K., Cai, X., Chen, D.J., Huang, L.H., Xiong, Y.Q. and Tan, S.Z. (2017b). Enhanced photocatalytic activity of Cu<sub>2</sub>O/g-C<sub>3</sub>N<sub>4</sub> heterojunction coupled with reduced graphene oxide three-dimensional aerogel photocatalysis. *Mater. Res. Bull.*, 96, 18-27. <http://doi.org/10.1016/j.materresbull.2016.12.009>
- Yang, C., Tan, Q.Y., Li, Q., Zhou, J., Fan, J.J., Li, B., Sun, J. and Lv, K.L. (2020a). 2D/2D Ti<sub>3</sub>C<sub>2</sub> MXene/g-C<sub>3</sub>N<sub>4</sub> nanosheets heterojunction for high efficient CO<sub>2</sub> reduction photocatalyst: Dual effects of urea. *Appl. Catal. B.*, 268, 118738. <http://doi.org/10.1016/j.apcatb.2020.118738>
- Yang, X.F., Chen, Z.P., Xu, J.S., Tang, H., Chen, K.M. and Jiang, Y. (2015). Tuning the morphology of g-C<sub>3</sub>N<sub>4</sub> for improvement of Z-scheme photocatalytic water oxidation. *ACS Appl. Mater. Interfaces*, 7(28), 15285-15293. <http://doi.org/10.1021/acsmami.5b02649>
- Yang, Y., Zhang, C., Huang, D.L., Zeng, G.M., Huang, J.H., Lai, C., Zhou, C.Y., Wang, W.J., Guo, H. and Xue, W.J. (2019). Boron nitride quantum dots decorated ultrathin porous g-C<sub>3</sub>N<sub>4</sub>: Intensified exciton dissociation and charge transfer for promoting visible-light-driven molecular oxygen activation. *Appl. Catal. B.*, 245, 87-99. <http://doi.org/10.1016/j.apcatb.2018.12.049>
- Yang, Y., Zeng, G.M., Huang, D.L., Zhang, C., He, D.H., Zhou, C.Y., Wang, W.J., Xiong, W.P., Song, B., Yi, H., Ye, S.J. and Ren, X.Y. (2020b). In situ grown single-atom cobalt on polymeric carbon nitride with bidentate ligand for efficient photocatalytic degradation of refractory antibiotics. *Small.*, 16, 2001634. <http://doi.org/10.1002/smll.202001634>
- Yang, Y., Li, X., Zhou, C.Y., Xiong, W.P., Zeng, G.M., Huang, D.L., Zhang, C., Wang, W.J., Song, B., Tang, X., Li, X.P. and Guo, H. (2020c). Recent advances in application of graphitic carbon nitride-based catalysts for degrading organic contaminants in water through advanced oxidation processes beyond photocatalysis: A critical review. *Water Res.*, 184, 116200. <http://doi.org/10.1016/j.watres.2020.116200>
- Yang, Y., Zeng, G.M., Huang, D.L., Zhang, C., He, D.H., Zhou, C.Y., Wang, W.J., Xiong, W.P., Li, X.P., Li, B.S., Dong, W.Y. and Zhou, Y. (2020d). Molecular engineering of polymeric carbon nitride for highly efficient photocatalytic oxytetracycline degradation and H<sub>2</sub>O<sub>2</sub> production. *Appl. Catal. B.*, 272, 118970. <https://doi.org/10.1016/j.apcatb.2020.118970>
- Ye, L.Q., Su, Y.R., Jin, X.L., Xie, H.Q. and Zhang, C. (2014). Recent advances in BioX (X= Cl, Br and I) photocatalysts: synthesis, modification, facet effects and mechanisms. *Environ. Sci. Nano*, 1(2), 90-112. <http://doi.org/10.1039/c3en00098b>
- Ye, S., Wang, R., Wu, M.Z. and Yuan, Y.P. (2015). A review on g-C<sub>3</sub>N<sub>4</sub> for photocatalytic water splitting and CO<sub>2</sub> reduction. *Appl. Surf. Sci.*, 358, 15-27. <http://doi.org/10.1016/j.apsusc.2015.08.173>
- Ye, S.J., Yan, M., Tan, X.F., Liang, J., Zeng, G.M., Wu, H.P., Song, B., Zhou, C.Y., Yang, Y. and Wang, H. (2019). Facile assembled biochar-based nanocomposite with improved graphitization for efficient photocatalytic activity driven by visible light. *Appl. Catal. B*, 250, 78-88. <http://doi.org/10.1016/j.apcatb.2019.03.004>
- Ye, S.J., Cheng, M., Zeng, G.M., Tan, X., Wu, H.P., Liang, J., Shen, M.C., Song, B., Liu, J.Q., Yang, H.L. and Zhang, Y.F. (2020). Insights into catalytic removal and separation of attached metals from natural-aged microplastics by magnetic biochar activating oxidation process. *Water Res.*, 179, 115876. <http://doi.org/10.1016/j.watres.2020.115876>
- Yi, H., Yan, M., Huang, D.L., Zeng, G.M., Lai, C., Li, M.F., Huo, X.Q., Qin, L., Liu, S.Y. and Liu, X.G. (2019). Synergistic effect of artificial enzyme and 2D nano-structured Bi<sub>2</sub>WO<sub>6</sub> for eco-friendly and efficient biomimetic photocatalysis. *Appl. Catal. B*, 250, 52-62. <http://doi.org/10.1016/j.apcatb.2019.03.008>
- Yuan, X.Y., Zhou, C., Jin, Y.R., Jing, Q.Y., Yang, Y.L., Shen, X., Tang, Q., Mu, Y.H. and Du, A.K. (2016). Facile synthesis of 3D porous thermally exfoliated g-C<sub>3</sub>N<sub>4</sub> nanosheet with enhanced photocatalytic degradation of organic dye. *J. Colloid Interface Sci.*, 468, 211-219. <http://doi.org/10.1016/j.jcis.2016.01.048>
- Zhang, G.G., Zhang, M.W., Ye, X.X., Qiu, X.Q., Lin, S. and Wang, X.C. (2014a). Iodine modified carbon nitride semiconductors as visible light photocatalysts for hydrogen evolution. *Adv. Mater.*, 26(5), 805-809. <http://doi.org/10.1002/adma.201303611>
- Zhang, J., Li, J.Y., Wang, W.P., Zhang, X.H., Tan, X.H., Chu, W.G. and Guo, Y.G. (2018). Microemulsion assisted assembly of 3d porous s/graphene@g-c<sub>3</sub>n<sub>4</sub> hybrid sponge as free-standing cathodes for high energy density li-s batteries. *Adv. Energy Mater.*, 8(14), 1702839. <http://doi.org/10.1002/aenm.201702839>
- Zhang, L.J., Li, S., Liu, B.K., Wang, D.J. and Xie, T.F. (2014b). Highly efficient CdS/WO<sub>3</sub> photocatalysts: z-scheme photocatalytic mechanism for their enhanced photocatalytic H<sub>2</sub> evolution under visible light. *ACS Catal.*, 4(10), 3724-3729. <http://doi.org/10.1021/cs500794j>
- Zhang, M., Jiang, W.J., Liu, D., Wang, J., Liu, Y.F., Zhu, Y.Y. and Zhu, Y.F. (2016a). Photodegradation of phenol via C<sub>3</sub>N<sub>4</sub>-agar hybrid hydrogel 3D photocatalysts with free separation. *Appl. Catal. B*, 183, 263-268. <http://doi.org/10.1016/j.apcatb.2015.10.049>
- Zhang, S.W., Li, J.X., Wang, X.K., Huang, Y.S., Zeng, M.Y. and Xu, J.Z. (2015). Rationally designed 1D Ag@AgVO<sub>3</sub> nanowire/graphene/protonated g-C<sub>3</sub>N<sub>4</sub> nanosheet heterojunctions for enhanced photocatalysis via electrostatic self-assembly and photochemical reduction methods. *J. Mater. Chem.*, 3(18), 10119-10126. <http://doi.org/10.1039/C5TA00635J>
- Zhang, X., Yang, P. and Jiang, S.P. (2021). Pt nanoparticles embedded spine-like g-C<sub>3</sub>N<sub>4</sub> nanostructures with superior photocatalytic activity for H<sub>2</sub> generation and CO<sub>2</sub> reduction. *Nanotechnology*, <http://doi.org/10.1088/1361-6528/abdcce>
- Zhang, Y.L., Zhang, H.J., Cheng, L.L., Wang, Y.J., Miao, Y., Ding, G.J. and Jiao, Z. (2016b). Two physical strategies to reinforce a non-metallic photocatalyst, g-C<sub>3</sub>N<sub>4</sub>: vacuum heating and electron beam

- irradiation. *Rsc. Adv.*, 6(17), 14002-14008. <http://doi.org/10.1039/c5ra22732a>
- Zhao, S., Huang, W.W., Wang, X.Q., Fan, Y.R. and An, C.J. (2019). Sorption of Phenanthrene onto Diatomite under the Influences of Solution Chemistry: A Study of Linear Sorption based on Maximal Information Coefficient. *J. Environ. Inform.*, 34(1), 35-44. <http://doi.org/10.3808/jei.201600329>
- Zhao, S., Fang, J.S., Wang, Y.Y., Zhang, Y.W., Zhou, Y.M. and Zhuo, S.P. (2020). Construction of three-dimensional mesoporous carbon nitride with high surface area for efficient visible-light-driven hydrogen evolution. *J. Colloid Interface Sci.*, 561, 601-608. <http://doi.org/10.1016/j.jcis.2019.11.035>
- Zhao, X., Guan, J., Li, J., Li, X., Wang, H., Huo, P. and Yan, Y. (2021). CeO<sub>2</sub>/3D g-C<sub>3</sub>N<sub>4</sub> heterojunction deposited with Pt cocatalyst for enhanced photocatalytic CO<sub>2</sub> reduction. *Appl. Surf. Sci.*, 537, 147891. <http://doi.org/10.1016/j.apsusc.2020.147891>
- Zheng, S., Cai, Y. and O'Shea, K.E. (2010). TiO<sub>2</sub> Photocatalytic Degradation of Phenylarsonic Acid. *J. Photochem. Photobiol. A. Chem.*, 210(1), 61-68. <http://doi.org/10.1016/j.jphotochem.2009.12.004>
- Zheng, Y., Lin, L.H., Ye, X.J., Guo, F.S. and Wang, X.C. (2014). Helical graphitic carbon nitrides with photocatalytic and optical activities. *Angew. Chem. Int. Ed.*, 53(44), 11926-11930. <http://doi.org/10.1002/anie.201407319>
- Zhou, B., Waqas, M., Yang, B., Xiao, K., Wang, S.Y., Zhu, C.Z., Li, J.Y. and Zhang, J.M. (2020a). Convenient one-step fabrication and morphology evolution of thin-shelled honeycomb-like structured g-C<sub>3</sub>N<sub>4</sub> to significantly enhance photocatalytic hydrogen evolution. *Appl. Surf. Sci.*, 506, 145004. <http://doi.org/10.1016/j.apsusc.2019.145004>
- Zhou, B.X., Ding, S.S., Zhang, B.J., Xu, L., Chen, R.S., Luo, L., Huang, W.Q., Xie, Z., Pan, A.L. and Huang, G.F. (2019a). Dimensional transformation and morphological control of graphitic carbon nitride from water-based supramolecular assembly for photocatalytic hydrogen evolution: from 3D to 2D and 1D nanostructures. *Appl. Catal. B.*, 254, 321-328. <http://doi.org/10.1016/j.apcatb.2019.05.015>
- Zhou, C.Y., Zeng, G.M., Huang, D.L., Luo, Y., Cheng, M., Liu, Y., Xiong, W.P., Yang, Y., Song, B. and Wang, W.J. (2020b). Distorted polymeric carbon nitride via carriers transfer bridges with superior photocatalytic activity for organic pollutants oxidation and hydrogen production under visible light. *J. Hazard. Mater.*, 386, 121947. <http://doi.org/10.1016/j.jhazmat.2019.121947>
- Zhou, C.Y., Xu, P., Lai, C., Zhang, C., Zeng, G.M., Huang, D.L., Cheng, M., Hu, L., Xiong, W.P., Wen, X.F., Qin, L., Yuan, J.L. and Wang, W.J. (2019b). Rational design of graphic carbon nitride copolymers by molecular doping for visible-light-driven degradation of aqueous sulfamethazine and hydrogen evolution. *Chem. Eng. J.*, 359, 186-196. <http://doi.org/10.1016/j.cej.2018.11.140>
- Zhou, J.J., Ji, X.H., Zhou, X.H., Guo, J., Sun, J.Y. and Liu, Y.C. (2018). Three-dimensional g-C<sub>3</sub>N<sub>4</sub>/MgO composites as a high-performance adsorbent for removal of Pb(II) from aqueous solution. *Sep. Sci. Technol.*, 54(17), 2817-2829. <http://doi.org/10.1080/01496395.2018.1553983>
- Zhou, L., Feng, J.R., Qiu, B.C., Zhou, Y., Lei, J.Y., Xing, M.Y., Wang, L.Z., Zhou, Y.B., Liu, Y.D. and Zhang, J.L. (2020c). Ultrathin g-C<sub>3</sub>N<sub>4</sub> nanosheet with hierarchical pores and desirable energy band for highly efficient H<sub>2</sub>O<sub>2</sub> production. *Appl. Catal. B*, 267, 118396. <http://doi.org/10.1016/j.apcatb.2019.118396>
- Zhou, X.R., Zeng, Z.T., Zeng, G.M., Lai, C., Xiao, R., Liu, S.Y., Huang, D.L., Qin, L., Liu, X.G. and Li, B.S. (2020d). Persulfate activation by swine bone char-derived hierarchical porous carbon: Multiple mechanism system for organic pollutant degradation in aqueous media. *Chem. Eng. J.*, 383, 123091. <http://doi.org/10.1016/j.cej.2019.123091>
- Zhou, Y.J., Sun, L.L., Wu, D.Y., Li, X., Li, J.Z., Huo, P.W., Wang, H.Q. and Yan, Y.S. (2020e). Preparation of 3D porous g-C<sub>3</sub>N<sub>4</sub> @V<sub>2</sub>O<sub>5</sub> composite electrode via simple calcination and chemical precipitation for supercapacitors. *J. Alloys Compd.*, 817, 152707. <http://doi.org/10.1016/j.jallcom.2019.152707>
- Zhou, Y.J., Zhang, L.X., Liu, J.J., Fan, X.Q., Wang, B.Z., Wang, M., Ren, W.C., Wang, J., Li, M.L. and Shi, J.L. (2015). Brand new P-doped g-C<sub>3</sub>N<sub>4</sub>: enhanced photocatalytic activity for H<sub>2</sub> evolution and Rhodamine B degradation under visible light. *J. Mater. Chem.*, 3(7), 3862-3867. <http://doi.org/10.1039/C4TA05292G>